Estrogen receptor α controls metabolism in white and brown adipocytes by regulating *Polg1* and mitochondrial remodeling

Zhenqi Zhou[1], Timothy M. Moore[1], Brian G. Drew[1], Vicent Ribas[1], Mete Civelek[2], Frode Norheim[2], Marcus M. Seldin[2], Alexander R. Strumwasser[1], Kate A. Whitney[1], Ellen Lester[1], Britany R. Reddish[1], Laurent Vergnes[2], Karen Reue[2], Prashant Rajbhandari[3], Peter Tontonoz[3], Jason Lee[4], Sushil K. Mahata[5], Sylvia C. Hewitt[6], Orian Shirihai[1], Craig Gastonbury[7], Kerrin S. Small[7], Markku Laakso[8], Jorgen Jensen[9], Sindre Lee[10], Christian A. Drevon[10], Kenneth S. Korach[6], Aldons J. Lusis[2], Andrea L. Hevener[1,11]

[1]Department of Medicine, Division of Endocrinology, Diabetes and Hypertension, [2]Department of Human Genetics [3]Department of Pathology and Laboratory Medicine and the Howard Hughes Research Institute, [4]Department of Molecular and Medical Pharmacology, David Geffen School of Medicine, University of California, Los Angeles, California USA 90095
[5]Department of Medicine, University of California, San Diego, La Jolla, California USA 92037
[6]Receptor Biology Section, NIEHS, NIH, Research Triangle Park, North Carolina USA 27709
[7]Department of Twin Research and Genetic Epidemiology, King's College London, London, UK
[8]Institute of Clinical Medicine, Internal Medicine, University of Eastern Finland and Kuopio University Hospital, Kuopio, Finland
[9]Department of Physical Performance, Norwegian School of Sport Science, Oslo, Norway
[10] University Department of Nutrition, Institute of Basic Medical Sciences, Faculty of Medicine, University of Oslo, Oslo, Norway
[11]Iris Cantor-UCLA Women's Health Research Center, Los Angeles, California USA 90095

Running title: ERα regulates mitochondrial metabolism in adipocytes

Corresponding author:
Andrea L. Hevener, Ph.D., University of California, Los Angeles, David Geffen School of Medicine, Division of Endocrinology, Diabetes, and Hypertension, 650 Charles E. Young Drive South, CHS Suite 34-115B, Los Angeles, California 90095-7073, Phone: (310) 794-7555 Fax: (310) 794-7654 E-mail: ahevener@mednet.ucla.edu

ABSTRACT

Objective: Abdominal adiposity and insulin resistance are heightened during aging and especially during the menopausal transition in women. Although the role of ERα in restraining adiposity and protecting against HFD-induced insulin resistance and obesity is well-established, the molecular mechanisms underlying ERα actions in adipocytes are inadequately understood.

Methods: We established the heritability of the ERα gene, *ESR1*, in adipose tissue by assessing fat biopsies from monozygotic twins of the UKTwins Study. We mined adipose tissue gene expression data from the METSIM Study of 700 Finnish men. Moreover, we interrogated the UCLA Hybrid Mouse Diversity Panel to understand the relationships between *Esr1* and other adipose tissue genes as well as the relationship between *Esr1* and complex traits including adiposity. To determine the mechanistic role of ERα in adipocytes we generated 2 adipose tissue-specific knockout mouse lines using the adiponectin and UCP1 Cre recombinase promoters to delete ERα from white and brown fat (FERKO and ERaKO^{BAT}, respectively). To interrogate the impact of ERα deletion on mitochondrial dynamics and function, we used a lentiviral-mediated approach to knockdown *Esr1* in 3T3-L1 adipocytes. ^{18}F-fluoro-2-deoxy-D-glucose micro positron emission tomography combined with computed tomography (^{18}F-FDG-PET/CT) after cold exposure (4 °C, 6h) was used to assess glucose uptake into BAT of Control$^{f/f}$ and ERaKO^{BAT} mice.

Results: We found strong *ESR1/Esr1* heritability in adipose tissue of female twins and both sexes of mice. From mouse to man, *Esr1/ESR1* expression was inversely associated with adiposity and positively associated with markers of metabolic health. In white adipose tissue, *Esr1* restrains Parkin-mediated elimination of mitochondria thus maintaining mitochondrial content and oxidative capacity. Indeed, adipose-selective Parkin KO mice have elevated mtDNA content and reduced adiposity. In brown adipocytes, *Esr1* is requisite for mitochondrial remodeling via Drp1 to promote Ucp1 induction and fatty acid mobilization during cold stress thermogenesis. In both white and brown adipocytes, alterations in mitochondrial remodeling and turnover appear consequent to a reduction in expression of the only mammalian mtDNA polymerase, *Polg1*.

Conclusions: Consistent with findings from other murine lines in which we selectively deleted *Esr1*, we find that ERα regulates mitochondrial dynamics and mitophagy via *Polg1*. ERα has strong heritability in adipose tissue and is essential for regulation of metabolic homeostasis and adiposity in males and females.

INTRODUCTION

Accumulation of excess fat underlies the development of obesity and metabolic dysfunction, and the clustering of metabolic abnormalities contribute to the development of chronic diseases including type 2 diabetes, cardiovascular disease and certain types of cancers (*1*). Although premenopausal women are less prone to metabolic diseases (*1*), this protection is lost during menopause and associated with a rapid increase in central adiposity (*1*). Striking new findings from the Study of Women's Health Across America (SWAN), show that during the menopausal transition (MT), beginning as early as 8 years prior to the final menstrual period (FMP), the mean rate of increase in fat mass in the average woman nearly doubles from 1%–1.7% per year, leading to a 6% total gain in fat mass over the 3.5 year–long MT analysis (*2*). The uniformly observed aging-associated rise in adiposity in both women and men is an important clinical outcome that requires improved mechanistic insight. In some studies a link between mitochondrial function and adiposity has been postulated (*3-6*), considering that mitochondria-related transcriptional signatures are downregulated in adipocytes of healthy monozygotic twins discordant for obesity (*3*). Moreover, ESR1 expression levels are reduced in fat from obese women (*7*). Although we have previously shown that selective deletion of ERα from adipocytes promotes increased adipocyte size and total adiposity in both male and female rodents (*8*), the mechanisms underlying these metabolic phenotypes remains inadequately understood. Because we have shown in other metabolic cell types that ERα directly controls mitochondrial DNA replication, fission-fusion remodeling and turnover, we determined the impact of ERα on mitochondrial function in white and brown adipocytes, and ascertain whether these molecular links established in rodents are relevant in humans.

Distinct from white adipose tissue, the major fat storage depot of the body, brown adipocytes are characterized by the ability to uncouple mitochondrial respiration from ATP synthesis to produce heat for the maintenance of body temperature (*9*). During cold exposure, mitochondrial remodeling is linked with the shift in substrate metabolism to fatty acid mobilization and the induction of uncoupling protein (UCP1) to produce heat (*10-16*). Considering that females possess increased abundance of brown adipose tissue (*17, 18*), brown adipose tissue is activated by estradiol treatment (*19*), and brown adipose tissue is enriched in mitochondria, we set out to determine the relationship between *Esr1* expression levels and adipose tissue metabolism. We sought to be the first to determine molecular mechanisms by which ERα regulates mitochondrial function specifically in brown adipocytes by studying a newly generated mouse model in which *Esr1* was selectively deleted in BAT.

In the current investigation we show that *ESR1* expression in fat is strongly heritable and that natural variation in adipose tissue *ESR1* expression is directly associated with markers of metabolic health. Since ERα is a transcription factor that predominantly resides in the nucleus we looked for ERα target genes that were coordinately dysregulated in both white and brown fat of ERα knockout mice. Through these tissue comparative studies we identified the mtDNA polymerase *Polg1* as the ERα target capable of controlling fission-fusion-mitophagy dynamics within two distinct fat cell populations. The impairment of the ERα-Polg1 axis led to cell-type specific effects on mitochondrial remodeling and turnover in white and brown adipocytes. In white adipocytes, ERα deletion heightened Parkin mediated-turnover of the mitochondrial genome and reduced oxidative capacity. Whereas in brown fat, reduced oxidative function was associated with impaired fission dynamics, blunted UCP1 activation, and diminished thermo-glucoregulatory capacity. Our findings confirm a conserved mechanism by which ERα controls a mitochondrial DNA replication–remodeling nexus to dictate metabolic flux and cellular health of adipose tissue.

RESULTS

Adipose tissue *ESR1* expression is inversely associated with adiposity and positively associated with insulin sensitivity

Human and mouse study overview is displayed in **Fig.1.** In adipose tissues biopsies from female monozygotic and dizygotic twin pairs (n=766, aged 38-85 years), TwinsUK study, the heritability for *ESR1* expression was 29%. In this cohort adipose tissue *ESR1* expression was inversely correlated with % fat mass (Bicor -0.308, P = 2.29E^{-09}) and plasma insulin (Bicor -0.025, P = 1.69E^{-05}). In dysglycemic (DG) men, a reduction in *ESR1* expression was observed in adipose tissue compared with normoglycemic (NG) controls (**Fig. 2A**). Following 90 days of exercise training, *ESR1* expression was increased in adipose tissue of NG men, whereas in contrast, *ESR1* expression remained unchanged from baseline in adipose tissue of DG men (**Fig. 2B**). Moreover, *ESR1* expression in adipose tissue from male participants in the MyoGlu study was inversely associated with visceral adipose tissue mass (**Fig. 2C**) and positively correlated to whole body insulin sensitivity (glucose infusion rate; GIR) as determined by glucose clamps (**Fig. 2D**). Similar relationships between adipose tissue *ESR1* expression and fat mass as well as the insulin resistance index HOMA-IR were observed in men participating in the much larger METSIM trial. Moreover, consistent with the relationship between adipose tissue *ESR1* being correlated with HOMA-IR, we also detected a strong inverse correlation between adipose expression of ESR1 and oral glucose tolerance (Bicor -0.36, P = 1.91x10^{-25}; 120 minute plasma glucose), insulin area under the curve (Bicor -0.409, P = 3.54x10^{-32}), and total triglyceride (Bicor -0.35, P = 1.22 x 10^{-23}). These findings in human subjects suggest that *ESR1* expression in adipose tissue is a strong surrogate marker of metabolic health. Similar to human subjects, in both male and female mice, adipose tissue *Esr1* expression was inversely correlated with the insulin resistance index HOMA-IR (**Fig. 2G-H**). Correlations between ESR1/Esr1 and all other genes in adipose tissue from METSIM, MyoGlu, and the HMDP were strikingly congruent, signifying fidelity of these datasets (**Fig. 2I**).

Similar to findings for human subjects, we observed a strong inverse relationship between adipose tissue Esr1 expression and fat mass in male and female mice of the HMDP (**Fig. 3A-B**). Thus, from mouse to man, there appears to be strong relationships between *ESR1* expression, adiposity, and insulin sensitivity. Since the male and female mice showed a similar relationship between Esr1 and adiposity, we looked at the overlapping, highly correlated Esr1 genes as determined by RNAseq analysis of fat from the HMDP (**Fig. 3C**). Of the 685 genes highly correlated with Esr1 (P<0.0001) in both sexes, none were discordant in the direction of correlation. The biological processes, i.e. GO terms, associated with the gene overlap include metabolic processes (**Fig. 3D**). To refine our understanding of ERα-regulated pathways in adipocytes and determine the molecular underpinnings contributing to the *Esr1*-adiposity relationship (**Fig. 3A-C**), we generated mice with a white (adiponectin Cre; FERKO) and brown adipose tissue (UCP1 Cre; ERαKO^{BAT}) ERα gene knockout. As previously shown by our group (*8*), we confirmed increased WAT mass (gonadal, gWAT; inguinal, iWAT) in both male and female FERKO mice (**Fig. 3E;** gonadal fat shown). Additionally as previously described, FERKO mice were hyperinsulinemic, hyperleptinemic, and glucose intolerant when fed a HFD compared with Control$^{f/f}$ (*8*). To determine the pathways disrupted by *Esr1* deletion and contributing to the increase in adiposity, we performed tissue gene arrays on gonadal white adipose tissue from FERKO and Control$^{f/f}$ mice. Functional annotation classification revealed significant enrichment scores (P < 0.01) for the mitochondria, nucleotide binding, transcription, DNA repair, helicase, and protein transport (**Fig. 3F**). Considering our numerous observations that ERα regulates mitochondrial function, dynamics and turnover in a variety of cell types (*20, 21*), we assessed the impact of ERα on mitochondrial function in white and brown fat.

ERα deficiency reduces Polg1 and mitochondrial DNA copy number in white adipose tissue

Although white adipocytes contain far less mitochondria than brown adipose, the most striking observation in adipose tissue from FERKO mice was the 70-80% reduction in mtDNA copy number in both females and males compared with ERα replete animals (**Fig. 3 G-H**). This observation is consistent with the findings of reduced mtDNA copy number in fat from obese and type 2 diabetic subjects (*22*). Next we assessed expression levels of standard markers of mitochondrial biogenesis and found that although no difference between the genotypes was observed for *Pgc1a*, *Tfam1*, or *Polg2*, a marked reduction in *Pgc1b*, *Nfr1*, *Polg1*, and *Polrmt* was observed in FERKO fat compared with Control$^{f/f}$ (**Fig. 3I-J**), suggesting that mitochondrial DNA replication and translation may be impacted by ERα deletion in adipocytes. Indeed, we confirmed a reduction in POLG1 total protein in FERKO fat (**Fig. 3 K-L**). Despite a marked reduction in mtDNA copy number, we did not detect a difference in the protein abundance of representative subunits of the electron transport chain in fat between the genotypes (**Fig. 3K**); this finding is similar to the observations made for ERα deficient vs. replete skeletal muscle (*20*).

To confirm a direct effect of ERα in adipocytes, we deleted *Esr1* from 3T3L1 adipocytes using a lentiviral shRNA approach (**Fig. 3M**). Similar to FERKO fat, we observed a reduction in mitochondrial DNA copy number and the gene that encodes for the mitochondrial DNA polymerase catalytic subunit *Polg1* in 3T3L1 adipocytes in culture (**Fig. 3N-P**). In addition, we also observed a marked reduction in three markers of mitochondrial biogenesis *Pgc1a*, *Tfam1*, and *Nrf1*, as well as substantial reductions in markers of the electron transport chain complexes, a finding contrasting with our observations in mice (**Fig. 3O-Q**). Since mtDNA replication is intimately linked with mitochondrial division, next we interrogated fission signaling. Internally consistent with a reduction in mtDNA copy number, the outer mitochondrial membrane docking protein FIS and phosphorylation of Drp1 at its activation site Ser616 were markedly reduced in Esr1-KD compared with ERα-replete adipocytes (**Fig. 3R-T**). These data suggest that adipocytes in culture may lack a specific compensatory homeostatic program present *in vivo* in adipose tissue.

ERα controls mitochondrial functionality and mitochondrial elimination by Parkin

Although the oxidative capacity of adipocytes is markedly lower than other insulin-responsive cell types, we determined whether ERα is essential for adipocyte oxygen consumption. Studies of real-time respirometry using Seahorse technology showed that when mitochondrial protein content was matched between the genotypes, respiratory capacity was remarkably reduced at basal and during maximally stimulated respiration in Esr1-KD adipocytes vs. ERα replete cells (**Fig. 4A**). In addition to reduced mtDNA copy number (suggestive of a loss of organelle number), the functional capacity of each organelle also appeared compromised. Consistent with these observations, fatty acid oxidation was reduced and reesterification was elevated in Esr1-KD cells vs. ERα replete (**Fig. 4B-C**). To understand the mechanisms contributing to the reduction in mtDNA copy number, we assessed mitophagic and mitochondrial dynamics (fission-fusion) signaling. Consistent with a reduction in mtDNA copy number, we observed an increase in PINK1 total protein and cleavage products as well as an increase in Parkin total protein in Esr1-KD adipocytes (**Fig. 4D-E**). The increase in Parkin protein was consistent with a reduction in Mfn2 protein (**Fig. 4F-G**), supporting its function to target outer mitochondrial membrane proteins for degradation to isolate mitochondria from the network promoting organelle turnover. To confirm the relationship between *Park2* (gene encoding Parkin) expression and adiposity *in vivo*, we determined that there is a strong positive correlation between the increase in adipose tissue Parkin expression for HF/HS:NC diets vs. the change in adiposity HF/HS:NC (**Fig. 4H;** $P = 0.026$). Next we performed fractionation studies to determine the localization of Parkin.

Although total protein was elevated in the lysate of Esr1-KD vs. Control (**Fig. 4D**), virtually no Parkin was detected in the cytosol; all was localized to the mitochondrial fraction of the adipocyte (**Fig. 4I**). These data suggest an enhanced signal for mitochondrial turnover or simply mitochondrial content elimination by Parkin in ERα-deficient adipocytes. Because p53 binds Parkin to regulate mitophagy (*23*) and p53 is a known ERα target shown to be induced with HFD-feeding and prevent beiging of white adipose tissue (*24, 25*), we followed this research line further. We found that the stress response protein, p53, was increased in the mitochondrial fraction of Esr1-KD cells and highly associated with Parkin (**Fig. 4I**). When we overexpressed *Esr1* in 3T3L1 adipocytes using adenovirus, the total expression of p53 and its localization to the mitochondria were diminished compared to control cells expressing only endogenous *Esr1* (**Fig. 4J**). Moreover, we chemically disrupted the binding of p53-Parkin by incubating cells with Pifithrin-α (PFT; 10-50 μmol/L for 5h). Inhibition of p53 led to nearly undetectable levels of Parkin in the mitochondrial fraction of adipocytes (**Fig. 4K-L**). These findings are consistent with the observation of increased mtDNA copy number and reduced adiposity in $p53^{-/-}$ (*25-27*), as well as $Parkin^{-/-}$ mice (**Fig. 4M-O**). Collectively these observations suggest a mechanism by which ERα controls the expression and localization of p53 and its binding partner Parkin, to control controlling adiposity (*24, 25*).

ERα controls macroautophagy in white adipose tissue to enhance mitophagy

Consistent with increased removal of unnecessary mitochondria, we observed that markers of macroautophagy required for mitochondrial turnover by the lysosome, including Beclin, Atg5, 7, 12, and LC3B processing, were all elevated in 3T3L1 adipocytes as well as mouse fat lacking ERα (**Fig. 5A-E**). Our findings support the notion that increased mitophagy may underlie the reduction in mtDNA copy number and the diminished oxidative metabolism in *Esr1*-deficient fat, and may explain the increased adiposity observed in women during aging (*2*).

ERα regulates UCP1 induction and substrate metabolism in brown adipocytes

Considering that females have increased brown adipose tissue and enhanced thermogenic capacity (*17, 18*), we hypothesized that Esr1 and Ucp1 expression levels would be higher in brown adipose tissue from females vs. males. Indeed we found that Esr1, Ucp1, and mitochondrial DNA copy number was increased in brown adipose tissue of WT female compared with male mice (**Fig. 6A & B**). Moreover, Esr1 expression was induced 4-fold during cold exposure (**Fig. 6C**) suggesting that ERα may play an important role in brown adipose tissue metabolism and thermoregulation. Importantly, *Esr1*, *Polg1*, and *Polg2* expression levels were reduced by HFD and genetic obesity/leptin deficiency (**Fig. 6D**). To understand the actions of ERα in brown adipocytes we used the UCP1 Cre recombinase mouse to generate animals with a BAT-selective Esr1 knockout (KO) (**Fig. 6E**). Consistent with this hypothesis, we observed a 50% reduction in Ucp1 expression in the basal state and a markedly blunted response of Ucp1 to cold challenge (6h at 4° C ; **Fig. 6F**). Reduced ERα expression in brown adipose tissue increased body weight gain and white adipose tissue accumulation during HFD (**Fig. 6G-H**). Brown adipose specific ERα KO mice, $ERaKO^{BAT}$, also showed reduced body temperature compared to $Control^{f/f}$ during the final stages of a cold tolerance test (**Fig. 6I**). To determine if there were differences in the BAT architecture we next performed histological analyses and found that BAT lacking ERα accumulated more and larger lipid droplets (**Fig. 6J).** We performed transmission electron microscopy and found that the mitochondria from $ERaKO^{BAT}$ mice were enlarged (increased mitochondrial perimeter and area) with thinner cristae (**Fig. 6 K-M**). In contrast to FERKO WAT, we observed no change in BAT mtDNA copy number between the genotypes for both sexes of mice (**Fig. 6N**). Similar to white adipose tissue of FERKO mice, we did observe a marked reduction of *Polg1* expression in $ERaKO^{BAT}$ compared with floxed controls (**Fig. 6O**). The maintenance of mtDNA copy number was internally consistent with matched

Parkin protein levels between the genotypes (**Fig. 6 P-Q**). As would be predicted, the accumulation of fat and change in mitochondrial morphology in BAT from ERaKO^{BAT} were paralleled by reduced fission signaling via Drp1 (**Fig. 6P, R, S**)(*28-30*). We previously observed *Polg1* reductions and mitochondrial fission incompetency in skeletal muscle and β-cells lacking ERα, thereby supporting a conserved mechanism by which ERα controls mitochondrial DNA replication and remodeling (*20, 21*). In the context of brown adipose tissue, Drp1 signaling to induce mitochondrial fragmentation is essential for lipid droplet utilization and Ucp1 induction during cold challenge, and thus requisite for effective thermoregulation (*30, 31*).

Esr1 deletion alters substrate metabolism in BAT during cold stress

Since we observed a blunted induction of Ucp1 and reduced mitochondrial fission signaling in BAT of ERαKO^{BAT}, we hypothesized that the increased lipid storage in the context of ERα deficiency was a consequence of impaired lipid mobilization and fatty acid oxidation. To test a shift in substrate reliance between the genotypes during cold stress we performed ^{18}FDG MicroCT-PET imaging following 6h cold challenge (4°C). Even at room temperature, BAT from ERαKO^{BAT} mice utilize more glucose than Control$^{f/f}$ (**Fig. 7A upper panels-B**), and this higher glucose reliance in ERαKO^{BAT} is further increased during cold stress when fatty acid oxidation is typically maximized (**Fig. 7A lower panels-B**). The increased reliance on glucose as fuel to maintain body temperature in ERαKO^{BAT} caused a marked reduction in blood glucose by ~50% during thermal challenge, whereas Control$^{f/f}$ maintained euglycemia even after 6h at 4°C (**Fig. 7C**). These findings suggest that in the absence of ERα, *Polg1* (a direct ERα target) is markedly reduced and mitochondria become dysfunctional either as a consequence of reduced mtDNA or because of an impaired capacity for mitochondrial remodeling. Aberrant mitochondrial remodeling/turnover underlies the accumulation of fat in both brown and white adipose tissue (**Fig. 7D**).

DISCUSSION

Our findings show that Esr1/ESR1 expression levels in adipose tissue have strong heritability and that natural expression in fat is inversely correlated with adiposity in males and females. Because mitochondrial content in fat, is reduced in obese and diabetic subjects (*3, 5, 32*), and since we have previously shown that ERα regulates mitochondrial function via fission-fusion-mitophagy dynamics (*20, 21*), we focused our efforts in this area. Our findings are consistent with a role for ERα in regulating adiposity by maintenance of mitochondrial DNA replication and mtDNA copy number. Females have higher expression levels of ERα in WAT and BAT than males and this is paralleled by higher mtDNA copy number as well as enhanced beiging/browning capacity. Brown adipose tissue activation is also elevated in females over males during cold challenge (*17, 18*). We showed that *Esr1* was induced by 4-fold in mouse BAT after a 6h cold challenge. In the context of ERα deletion, we noted a very striking reduction in mtDNA copy number in both male and female WAT compared with ERα replete animals. This is consistent with adipose tissue mtDNA depletion shown in rodent models of obesity and type 2 diabetes (*32*). Expression levels of the mtDNA polymerase *Polg1* and the mtRNA polymerase *Polrmt* as well as transcription factors associated with mitochondrial biogenesis *Pgc1b* and *Nrf1*, were all reduced in adipose tissue lacking ERα. Similar reductions in *Polg1*, mtDNA copy number and genes associated with mitochondrial biogenesis were also observed in 3T3L1 adipocytes with Esr1-KD. As expected, we observed reduced cellular respiration and fatty acid oxidation in adipocytes lacking ERα.

Because the reduction in mtDNA copy number was so pronounced, we examined whether a loss of ERα promoted enhanced mitophagy signaling. Indeed, we observed a strong increase in the ERα-regulated mitochondrial stress signal p53 (*33*), as well as the E3 ubiquitin ligase Parkin.

Both p53 and Parkin were coordinately recruited to the mitochondria in Esr1-KD cells. When we overexpressed Esr1 in adipocytes, mitochondrial p53 and Parkin were reduced compared with control cells. When we chemically inhibited p53 using PFTα, we observed a striking reduction in p53 as well as Parkin in the mitochondrial fractions. Moreover when we used conventional genetics to inactivate Parkin in adipose tissue, we observed increased mtDNA copy number and reduced white adipose tissue mass. Interestingly p53 is increased in WAT of aged, high fat diet-fed, and genetically obese mice, and is associated with insulin resistance (*24, 25, 27, 34*). Our findings are consistent with published findings on p53 and Parkin inhibition blocking mitophagy, increasing mtDNA content, and enhancing beiging capacity of WAT (*24, 35, 36*). Moreover, both the p53 and Parkin KO mice, and now herein the adipose-specific Parkin KO, show reduced WAT accumulation on a normal chow diet and following HFD-feeding (*25, 26, 37*). Parkin inhibition promotes prolonged retention of beige adipocytes even after β3-AR agonist withdrawal (*38*). Furthermore, WAT has a higher mitophagic activity compared with BAT and a low spare respiratory capacity; thus a blunted mitochondrial activity compared with beige and brown adipocyes (*38*). Parkin-mediated mitophagy is selectively downregulated during browning of WAT (*36*). These findings suggest that the WAT beiging phenomenon during ERα agonism observed by Santos et al. (*39*), may be underpinned by suppression of the p53-Parkin axis to remodel/turnover the mitochondrial network. Our laboratory is currently interrogating whether transient conditional overexpression of Esr1 restrains HFD feeding-induced increases in adiposity.

It is also of interest to note the striking differences in mitochondrial DNA content between brown, beige, and WAT as well as the striking sex differences in BAT abundance and activity (*17, 31, 40*). Because females have higher BAT abundance and increased BAT activation, we examined whether ERα may play a role in regulating BAT metabolism. We showed that BAT from females expresses higher levels of basal *Esr1* and *Ucp1* as well as mtDNA copy number compared with males. During cold exposure (4°C for 5h) Esr1 is induced ~4fold. To test the role of ERα in BAT we used the Ucp1 Cre mouse line crossed into the floxed Esr1 mouse line to generate animals with a BAT-selective ERα deletion. Despite generating only a modest 50% reduction in ERα protein, we found that induction of Ucp1 following cold exposure was completely blunted in mice with ERα-deficient BAT. Moreover, these mice were more susceptible to adipose tissue weight gain and showed impaired thermoregulatory capacity. Brown adipose tissue from animals lacking ERα also showed marked accumulation of lipid as the droplets were larger and more abundant. Mitochondria from ERα-deficient BAT were also enlarged with thinner cristae. Similar to the reduction in *Polg1* in WAT of male and female FERKO mice, *Polg1* was also reduced by ~70% in BAT of ERaKO^{BAT}. This finding is consistent with our previous studies in skeletal muscle showing a direct role for ERα in the regulation of Polg1 expression and mtDNA replication (*20*). Despite the reduction in Polg1 expression in BAT of ERaKO^{BAT}, in contrast to FERKO, mtDNA copy number was maintained when compared to control ERα replete BAT. This is consistent with reduced mitophagic capacity of BAT vs WAT as previously described (*36, 38*). In contrast to our findings of elevated Parkin in WAT from FERKO mice, we observed no difference in Parkin protein expression in BAT between the genotypes. Overall, our observations in ERα-deficient BAT regarding preservation of mtDNA copy number despite reduced mitochondrial DNA replication and impaired Drp1 signaling are reminiscent of findings in ERα-deficient skeletal muscle (*20*). Considering Forner et al. show that brown fat transcript and proteome are more similar to their counterparts in skeletal muscle than WAT (*40*) and that muscle and brown adipose tissue are derived from the same precursor lineage (*41-43*), our comparative observations between mouse models appears supported.

Because there was increased size and abundance of lipid droplets in BAT of ERaKO^{BAT} mice we tested if mitochondrial dysfunction may underlie a shift in substrate reliance. Brown adipose tissue activation and increased mitochondrial uncoupling are paralleled by increased Drp1 phosphorylation (*44, 45*), mitochondrial fission, increased respiration by complex II and a shift in substrate preference to fatty acids (*16, 29, 31, 46*). Previous reports show that activation of mitochondrial fission signaling by Drp1 was increased in brite and brown over white adipocytes (*31*). Moreover, knockdown of Drp1 to ~50% of baseline reduced Ucp1 expression and blunted uncoupled mitochondrial respiration (*31*). Our findings in BAT of ERaKO^{BAT} are congruent with these observations, as we showed ~50% reduction of Drp1 total protein and phosphorylation paralleled by increased reliance on glucose as opposed to fatty acids during cold challenge. We have previously shown that ERα expression is intimately connected with Polg1 expression and Drp1 signaling/fission competency (*20, 21*). Fission competency also appears requisite for mitochondrial DNA replication (*47*). We have observed that this axis exerts a strong feedback to control macro- and micro-autophagy and the balance of these control arms, mtDNA replication vs. degradation, appears to dictate the copy number of the mitochondrial genome in a cell type-specific manner (*48, 49*). Ongoing studies in our laboratory are focused on understanding whether ERα regulates *Polg1* similarly in all metabolic cell types and how *Polg1* controls mitochondrial DNA copy number, fission-fusion dynamics, and metabolic homeostasis *in vivo*.

Our findings support the notion that ERα regulates mitochondrial function and energy homeostasis in white and brown adipose tissue via coordinated control of mitochondrial DNA replication by Polg1 and by fission-fusion-mitophagy dynamics. Reduction of ERα action impairs mitochondrial function, promotes increased adiposity, and disrupts metabolic homeostasis in mouse and man. Therefore novel strategies to maintain ERα action in adipose tissue are attractive from a therapeutic standpoint to restrain adipose tissue weight gain and the development of metabolic dysfunction especially in women during the menopausal transition.

MATERIALS and METHODS

Human studies

TwinsUK. The narrow sense heritability (h2) of *ESR1* in adipose tissue was determined by accessing the data from the TwinsUK study in which subcutaneous adipose tissue from punch biopsies (8mm) were obtained adjacent and inferior to the umbilicus in ~766 healthy female monozygotic and dizygotic twins age 38-85 years (median age 62, ~75% postmenopausal by FMP calculation) (*50, 51*). Biopsies were RNAsequenced as described (*52*), and correlations between adipose tissue expression of ESR1 and metabolic traits were determined. TwinsUK RNAseq data is available from EGA (Accession number: EGAS00001000805). (**Fig. 1A**).

Skeletal Muscles, Myokines and Glucose Metabolism (MyoGlu). Between the years of 2011-2012, 26 sedentary (<1 exercise session/week) men of Scandinavian origin from Oslo, Norway (aged 40-65 years), were recruited into the Skeletal Muscles, Myokines and Glucose Metabolism (MyoGlu) intervention trial and divided into two groups: 1) normoglycemic (control) with BMI <27 kg/m^2 (n = 13), or 2) dysglycemic (DG) with BMI 27-32 kg/m^2 and either impaired fasting plasma glucose, impaired glucose tolerance or insulin resistance (based on HOMA-IR) (n=13). Exclusion criteria were family history of diabetes (for controls only), hypertension, liver or kidney disease, chronic inflammatory diseases, or on any medication expected to affect glucose metabolism (lipid lowering, anti-hypertensive, ASA, corticosteroids, etc.). As described previously (*53-56*), both groups underwent combined strength- and endurance training for 12w, including 2 endurance bicycle sessions (60 min) and two whole-body strength training sessions (60 min) per week. A 45min bicycle test at 70% of VO_2 max was performed before and after the 12w training period. Subcutaneous abdominal adipose tissue (n=48) were obtained 1h after acute bicycle test, before and after training. Biopsies were obtained from the periumbilical

subcutaneous tissue. After sterilization, the subcutaneous and superficial tissues were injected with Xylocain-adrenaline 10 mg/mL + 5 µg/mL. A 6 mm muscle biopsy needle (Pelomi, Albertslund, Denmark) was used with a 50 mL syringe for vacuum generation. Biopsies were quickly rinsed in cold PBS and dissected on a cold aluminium plate to remove blood before freezing. The MyoGlu study design is presented in **Fig. 1B**.

Metabolic Syndrome in Men (METSIM). For the study of adipose tissue insulin sensitivity (Study 1), 8,460 non-diabetic participants from an ongoing population-based cross-sectional Metabolic Syndrome in Men (METSIM) study [16, 17] were included. Participants, aged 45-70 years, were randomly selected from the population register of Kuopio, Eastern Finland (population 95,000). Of those included, 2,951 participants had normal glucose tolerance, 4,181 isolated impaired fasting glucose (IFG), 302 isolated impaired glucose tolerance (IGT), and 1,026 IFG and IGT according to American Diabetes Association criteria [18]. For the genetic association study (Study 2), the first 6,733 non-diabetic men (age 57.0 ± 6.9 years, BMI 26.8 ± 3.8 kg/m^2; mean ± SD) examined in the METSIM study were included. The gene expression study (Study 3) included 41 obese participants (age 44.2 ± 8.3 years, BMI 45.5 ± 6.1 kg/m^2 and 18 type 2 diabetic patients from an ongoing study, including participants undergoing bariatric surgery at the Kuopio University Hospital. All studies were approved by the ethics committee of the University of Kuopio and Kuopio University Hospital, and were carried out in accordance with the Helsinki Declaration. A 2 h OGTT (75 g glucose) was performed and samples for plasma glucose, insulin and NEFA were drawn at 0, 30 and 120 min. Plasma glucose was measured by enzymatic hexokinase photometric assay (Konelab System Reagents; Thermo Fischer Scientific, Vantaa, Finland); plasma insulin by immunoassay (Advia Centaur Insulin IRI, number 02230141; Siemens Medical Solutions Diagnostics, Tarrytown, NY, USA); serum NEFA by enzymatic colorimetric method (Konelab 20XTi Clinical Chemistry Analyzer; Thermo Fischer Scientific); HDL-cholesterol by enzymatic colorimetric test (Konelab System Reagents); and alanine aminotransferase (ALT) and total triacylglycerol by standard methods. Body composition was determined by bioelectrical impedance (Bioimpedance Analyzer Model BIA101; Akern Srl, Florence, Italy) with participants in the supine position after a 12 h fast [19]. Tissue-specific expression data were obtained from GeneSapiens [20], version IST4, containing expression data from 15 liver and 16 adipose tissue samples from healthy human tissue, measured with Affymetrix (Santa Clara, CA, USA) gene expression microarrays. METSIM adipose array data are available from GEO (GSE70353)(*57*). Gene-trait relationships presented herein were obtained from 770 male subjects (**Fig. 1C**).

Animals

Hybrid Mouse Diversity Panel (HMDP)

All mice were obtained from The Jackson Laboratory and bred at University of California, Los Angeles. Mice were maintained on a chow diet (Ralston Purina Company) until 8 weeks of age when they either continued on the chow diet or received a high fat/high sucrose diet (HF/HS Research Diets D12266B; 8 weeks) with the following composition: 16.8% kcal protein, 51.4% kcal carbohydrate, 31.8% kcal fat. A complete list of the strains included in this study is in **supplemental table s1**. This resource was established to provide a platform for high resolution genome wide mapping and systems level analysis of gene-gene and gene-trait relationships (**Fig. 1D**).

Genetically engineered mice

ERα floxed mice (Gift from Kenneth Korach) were crossed with adiponectin (Gift from Phillip Scherer) or UCP1 Cre mice (The Jackson Laboratory) to generate animals with ERα deletion in white and brown, or brown adipose tissue selectively (**Fig. 1E**). Whole body Parkin null mice (The Jackson Laboratory) and adipose-tissue selective Parkin knockout mice (Floxed Parkin

mice were a gift from Ted Dawson and these animals were crossed into the adiponectin Cre line) were used to confirm a role for Parkin in mediating the effects of ERα deletion on the mtDNA copy number. Mice were studied under normal chow (NC) and high fat diet (HFD)-fed conditions between the ages of 4-10 months. Mouse sex is indicted in the Figure Legends for each specific experiment.

Immunoblot analysis

Whole quadriceps muscles from both legs were pulverized together into a powder while frozen in liquid nitrogen and a homogenous sample of pulverized muscle was used for immunoblotting (*58*). Proteins from each individual whole cell homogenate were normalized (expressed relative to the pixel densitometry) to glyceraldehyde 3-phosphate dehydrogenase (GAPDH, AM4300, Ambion). Phosphorylation-specific proteins were normalized (expressed relative to pixel densitometry) to the same unphosphorylated protein (i.e. phosphorylated Drp1 at Ser 616 was expressed relative to the pixel densitometry of Drp1 for each individual sample). Primary antibodies included: Mitochondrial Fission Protein 1 (Fis1, GTX111010, GeneTex), Mitochondrial fission factor (MFF, ab81127, Abcam), Mitofusin 1 (MFN1, 75-162, NeuroMab), Mitofusin2 (MFN2, ab56889, Abcam), Transcription factor A, Mitochondrial (TFAM, ab131607, Abcam), Dynamin-related protein 1 (Drp1, 8570, Cell Signaling), phosphorylated Drp1 Ser616 (4494, Cell Signaling), phosphorylated Drp1 Ser637 (6319, Cell Signaling), OxPhos Complex I to V (ab110413, Abcam), Optic atrophy 1 (Opa1, 612606, BD Biosciences), PTEN Induced Putative Kinase 1 (Pink1, 10006283, Cayman Chemical), Parkin (2132, Cell Signaling), phosphorylated Parkin Ser65 (ab154995, Abcam), Microtubule-associated proteins 1A/1B light chain 3B (LC3B, 2775, Cell Signaling), Sequestosome 1 (p62, 5114, Cell Signaling), Beclin-1 (3738, Cell Signaling), Autophagy Related 7 (ATG7, 8558, Cell Signaling), Protein Kinase A (PKA, 4782, Cell Signaling), Autophagy Related 10 (ATG10, PA5-20454, ThermoFisher), phospho-AMPKα Thr172 (50081, Cell Signaling), PGC1α (2178, Cell Signaling), and phospho-PKA Thr197 (5661, Cell Signaling). In some cases immunoblots were stripped and re-probed with a different antibody, thus loading controls in specific instances were duplicated.

DNA & RNA extraction, cDNA synthesis, quantitative RT-PCR, and microarrays

DNA and RNA were extracted from a portion of frozen adipose tissue homogenate using DNeasy/RNeasy isolation kits (Qiagen) as described by the manufacturer. Isolated DNA and RNA were tested for concentration and purity using a NanoDrop Spectrophotometer (Thermo Scientific). Isolated RNA was converted into cDNA, checked for purity, and qPCR of the resulting cDNA levels was performed (*58*). All genes were normalized to the housekeeping gene Ppia or 18S. Mitochondrial DNA content was assessed as a ratio of mitochondrial DNA (mtCO2) to nuclear DNA (SDHA). See **supplemental table s2** for a list of qPCR primers.

Total RNA from HMDP mouse muscle (211 females, 228 males) was hybridized to Affymetrix HT_MG-430A arrays and scanned using standard Affymetrix protocols. To reduce spurious association, RMA normalization was performed after removing all individual probes with SNPs and all probesets including 8 or more SNP-containing probes, resulting in 22,416 remaining probesets. To determine the accuracy of microarray data, qPCR was used to test the expression of a dozen genes. A correlation of $r = 0.7$ between qPCR and microarray was determined. Frozen human adipose tissue biopsies were cooled in liquid nitrogen and crushed to powder by a pestle in a liquid nitrogen-cooled mortar as described by Langleite et al. (*55*). Frozen biopsies were transferred into 1 mL QIAzol Lysis Reagent (Qiagen, Hilden, Germany), and homogenized using TissueRuptor (Qiagen) at full speed for 15 sec, twice. Total RNA was isolated from the homogenate using RNeasy Mini Kit (Qiagen). RNA integrity and concentration were determined using Agilent RNA 6000 Nano Chips on a Bioanalyzer 2100 (Agilent Technologies Inc, Santa Clara, CA). Using High-Capacity cDNA Reverse Transcription Kit (Applied Biosystems, Foster,

CA), 200 ng of total RNA was converted to cDNA for TaqMan real-time RT-PCR. The cDNA reaction mixture was diluted in water and cDNA equivalent of 25 ng RNA used for each sample. Quantitative real-time PCR was performed with reagents and instruments from Applied Biosystems in the 96-well format using a 7900HT Fast instrument and the SDS 2.3 software (Applied Biosystems). Relative target mRNA expression levels were calculated as $2^{-\Delta Ct}$, and normalized to beta-2 microglobulin (B2M, Hs00984230_m1) (*59*). mRNA sequencing was performed using the Illumina HiSeq 2000 system (Illumina, San Diego, CA). cDNA sequenced read alignment was carried out using Tophat v2.0.8. Reads counted by gene feature were performed by featureCounts in Rsubread 1.14.2.

Tissue histology

Gonadal adipose tissue pads from Control and both white and brown adipose tissue ERαKO models were fixed in formalin, sectioned and stained as previously described (*8, 60*). Adipocyte nuclei and total adipocyte number and size were counted or measured using ImageJ software.

Mitochondrial isolation

Mitochondria were isolated from gastrocnemius muscle using a Dounce homogenizer and Mitochondria Isolation Kit for Tissue (Thermo Scientific) with a Percoll density method for added purification (*61*). Briefly, gastrocnemius muscles were washed in ice-cold PBS, Dounce homogenized, and centrifuged at 800g for 10 min at 4°C. The supernatant was centrifuged at 12,000g for 15 min at 4°C. The pellet was washed and purified using isolation buffer and Percoll solution. Isolated mitochondria were mixed with lysis buffer (200 uL, 12 mM sodium lauroyl sarcosine, 0.5% sodium deoxycholate, 50 mmol/L triethylammonium bicarbonate (TEAB)), then subjected to bath sonication for 10 min (Bioruptor Pico, Diagenode Inc., Denville, NJ, USA) and heated (95°C for 5 min).

Real-time respirometry of adipocytes

Control (Scr) and Esr1-KD 3T3-L1 fibroblasts were seeded in 24-well Seahorse plates (Seahorse Biosciences) and differentiated to adipocytes. Mitochondrial respiration in adipocytes was measured using an XF24 Extracellular Flux Analyzer (Seahorse Biosciences, North Billerica, MA). Measurements of oxygen consumption were made continuously while cells were sequentially treated with oligomycin (ATP synthase inhibitor), FCCP (an uncoupling agent), and rotenone/myxothiazol (inhibitors of complex I/III of the electron transport chain)(*21*).

FDG positron emission tomography-computed tomography imaging

PET tracers, ^{18}F-FDG and ^{18}F-DFA, were synthesized as previously described (*62*). ^{18}F-FDG was obtained from the UCLA Translational Imaging Division. Mice were injected with ExiTron nano 12,000 (100μL), 3d before the PET imaging experiment. Mice were anesthetized, injected with approximately 2.96 MBq of ^{18}F-FDG (after overnight fast) or ^{18}F-DFA, and after 60 min imaged for 10 min on a G8 PET/CT (SOFIE Biosciences). Different cohorts of mice were used for the room temperature vs. cold tolerance testing (4°C for 4h) studies. A blinded observer, unaware of the intervention groups, performed the PET quantification using only the CT image to examine the regions of interest. ^{18}F-DFA and ^{18}F-FDG accumulation were normalized to the respective accumulation in the brain and right forelimb triceps. Brain was used as a reference region for the quantification of ^{18}F-DFA accumulation as specific accumulation of ^{18}F-DFA in the brain has never been observed, and the same brain region could be readily identified and quantified across individual animals. Image-derived blood ^{18}F-DFA levels were quantified from the left ventricle. Hepatic ^{18}F-DFA contrast, correlation, and entropy were determined using the GLCM Texture plugin in ImageJ (version 1.50i) (*63*).

Statistical analyses

Values are presented as means ± SEM and expressed relative to the respective control group. Group differences were assessed by one-way ANOVA followed by Tukey Honest Significant Difference *post hoc* test, Student's t-test, or two-way ANOVA where appropriate. Venn Diagram was created using the VennDiagram package (Version 1.6.20) in R Studio. ESR1/Esr1 by gene correlations were calculated in adipose tissue from METSIM, MyoGlu, and HMDP studies using the mid-weight bicorrelation function in the WGCNA package (Version 1.67) in R Studio. Significant correlations were set as $P<0.0001$. Gene symbols from the HMDP were converted to human orthologs using biomaRt package (Version 2.38.0) in R Studio. For all other comparisons, statistical significance was established *a priori* at $P < 0.05$ (Graph Pad Prism 7.0).

AUTHOR CONTRIBUTIONS

Conceived and designed the experiments: ALH, ZZ, TMM, JL, MMS, KS, ML, PT, KS, ML, AJL, OS, KSK, CAD, SL, KR, FN, and CAD. Performed the experiments: ZZ,TMM, VR, BGD, PR, MC, FN, MMS, KAW, EL, BRR, JJ, CG, LV, PR, SKM, SCH, JL, and SL. Analyzed the data: ZZ, TMM, VR, PR, BGD, MC, KAW, LV, SKM, SCH, SL, KS, ML, SL, MMS, and FN. Wrote the manuscript: ZZ, BDG, OS, CAD, OS, CAD, KSK, AJL, and ALH.

ACKNOWLEDGMENTS

We would like to thank Kåre I. Birkeland (Oslo University Diabetes Research Centre), Calvin Pan (UCLA Department of Human Genetics), UCLA Division of Laboratory Animal Medicine, and Pamela Berryhill and Katie Moore for assisting us in data collection, animal welfare, and the preparation of this manuscript respectively. This research was supported in part by the UCLA Department of Medicine, The UCLA Iris Cantor Women's Health Center Research Foundation and UCLA CTSI (ULTR000124), The UCLA Claude D. Pepper Older Americans Independence Center, and the National Institutes of Health (DK109724, P30DK063491, and NURSA NDSP to ALH under parent award U24DK097748). ZZ was supported by UCLA Claude Pepper Older Americans Independence Center funded by the National Institute of Aging (5P30AG028748), NIH/NCATS UCLA CTSI Grant (UL1TR000124), and UCLA Center for Duchenne Muscular Dystrophy-NIH NIAMS (U54 AR052646) Wellstone Center of Excellence Training TMM was supported by a Kirschstein-NRSA predoctoral fellowship (F31DK108657), a Carl V. Gisolfi Memorial Research grant from the American College of Sports Medicine, and a predoctoral graduate student award from the Dornsife College at the University of Southern California. SKM was supported by a grant from the Department of Veterans Affairs (I01BX000323). Research was supported by the NIEHS Division of Intramural Research 1ZIAES070065 to KSK. AJL was supported by NIH grants HL28481 and HL30568. KR, AJL, and ALH are collaboratively supported by an NIH SCORE on Sex Differences and Women's Health (U54DK120342).

The MyoGlu trial is registered at ClinicalTrail.gov; NCT01803568. This work was supported by grants from the Institute of Basic Medical Sciences, UiO, Johan Throne-Holst Foundation for Nutrition Research, Freia Medical Research Foundation, the "Functional Genomics" and "Infrastructure" programs of the Research Council of Norway and the Southeastern Regional Health Authorities and EU-financed FP7 project (NutriTech grant agreement no: 289511). We thank Anne Randi Enget, Ansgar Heck and Birgitte Nellemann for taking the biopsies, and Tor I Gloppen, Torstein Dalen, Håvard Moen, Marius A Dahl, Guro Grøthe, Egil Johansen, Katrine A Krog, Øyvind Skattebo, Daniel S Tangen, Kristoffer K Jensen, Hans K Stadheim, and Eirin Rise for conducting the human strength and endurance intervention (MyoGlu) under supervision of Professor Jørgen Jensen. Sequencing was performed by PhD Gregor Gilfilan at the Norwegian Sequencing Centre (www.sequencing.uio.no) in collaboration with Torgeir Holen supported by the Research Council of Norway and the South-eastern Regional Health Authorities.

The METSIM studies were supported by grants from the Academy of Finland (contract 124243), The Finnish Heart Foundation, The Finnish Diabetes Research Foundation, TEKES (contract 1510/31/06), EVO grants (5232 and 5263) and the Commission of the European Community (contract LSHM-CT-2004_512013 EUGENE2).

TwinsUK – The TwinsUK study was funded by the Wellcome Trust and European Community's Seventh Framework Programme (FP7/2007-2013). The TwinsUK study also receives support from the National Institute for Health Research (NIHR) – funded Bioresource, Clinical Research Facility and Biomedical Research Centre based at Guy's and St Thomas' NHS Foundation Trust in partnership with King's College London.

CONFLICT OF INTEREST

The authors declare no competing financial interests in relation to this research.

APPENDIX A. SUPPLEMENTARY DATA

FIGURE LEGENDS

Fig. 1. Schematic overview of the human and mouse studies in this investigation.
(A) UK Twins, a study of ~766 healthy female monozygotic twins ages 38-85 years (median age 62, ~75% postmenopausal by FNP calculation). Adipose tissue samples were harvested and gene expression was determined by RNAsequencing. (B) MyoGlu exercise (two endurance and 2 strength training sessions, 60 min each, 4 x per week) studies in 13 normoglycemic (NG) and 13 dysglycemic (DG) men (age 45-60 years), with adipose tissue samples excised prior to and after training. (C) METSIM studies in Finnish men (n=8,460) age 45-70 years included adipose tissue gene expression determined by Affymetrix microarrays and correlated with complex traits in n=770 subjects. (D) Studies in the UCLA Hybrid Mouse Diversity Panel (HMDP) comprised of 100 inbred and recombinant inbred male and female mice under normal chow (NC) and high fat-high sucrose (HF-HS) diet in the sedentary condition (4 mice per strain / per condition; 12 weeks of age). (E) Studies in male and female white (WAT) and brown (BAT) adipose tissue-specific ERα knockout mice, FERKO and ERαKO^{BAT}

Fig. 2. Adipose tissue *ESR1/Esr1* expression is strongly associated with adiposity and insulin sensitivity. (A) ESR1 expression is reduced in adipose tissue of dysglycemic men (DG; closed bar) compared with normoglycemic men of the MyoGlu study (n=13 NG Controls and n=11 DG; age 40-65y). (B) Adipose tissue *ESR1* expression is increased in normoglycemic men following exercise training whereas no change in adipose *ESR1* expression from sedentary was observed for dysglycemic men. (C-D) Adipose tissue *ESR1* expression is inversely correlated with visceral adipose tissue and directly correlated with insulin sensitivity as assessed by the glucose clamp technique glucose infusion rate (GIR). (E-F) Similar to the findings of MyoGlu, adipose tissue *ESR1* expression was inversely correlated with fat mass (%) and the insulin resistance index HOMA-IR in men from the METSIM study (n=770 men, age 45±70 years). (G-H) Esr1 expression in gonadal adipose tissue from (G) male and (H) female HMDP mice (4 mice/strain, ~100 strains/sex). (I) Venn diagram depicting overlap in ESR1/Esr1 by gene correlations (mid-weight bicorrelation) in adipose tissue from METSIM, MyoGlu, and HMDP studies. Data are means ± SEM. *, $P<0.05$. Mean differences were detected using Student's t-test for correlated groups and repeated measures ANOVA where appropriate. Correlations were determined using linear regression analysis, Pearson's r.

Fig. 3. ERα deficiency reduces *Polg1* and mitochondrial DNA copy number in white adipose tissue. (A-B) Natural expression of *Esr1* in adipose tissue of male and female mice of the HMDP (each dot represents a different mouse strain, n = X/strain). (C) We identified 685 Esr1 correlated genes ($P < 0.0001$) in WAT of the male and female HMDP, and (D) these overlapping and highly correlated Esr1 genes represent a variety of metabolic processes. (E) Gonadal adipose tissue weight was elevated in mice lacking ERα in fat. (F) Functional annotation analysis of the processes disrupted by adipose tissue ERα deletion include mitochondrion,

nucleotide binding, transcription, DNA repair, helicase, and protein transport. (G-H) mtDNA copy number is reduced in adipose tissue from male and female FERKO mice (n=6-8 mice/genotype). (I) *Pgc1b* and *Nrf1* are reduced while *Pgc1a* and *Tfam1* are maintained in expression in fat from female FERKO mice (n=6/genotype). (J-L) *Polg1* mRNA and protein, representing the catalytic subunit of the mtDNA polymerase POLG, are markedly reduced in female FERKO fat (n=6 mice/genotype), as was the expression of the mitochondrial RNA polymerase *Polrmt*. (M) Esr1 was deleted in 3T3L1 adipocytes and similar to FERKO this led to a reduction in (N) mtDNA copy number as well as (O) markers of mitochondrial biogenesis including *Pgc1a, Nrf1, Tfam*, (P) *Polg1 and Polg2* (n=3 in triplicate), and (Q) representative subunits of the electron transport chain (n=3 in triplicate/condition). (R-T) Esr1-KD reduced mitochondrial fission signaling via diminished FIS and p-Drp1^{Ser616} in Esr1-KD vs. Control (Scr) 3T3L1 adipocytes (n=3/group in duplicate). *, $P<0.05$ between the genotypes. Mean ± SEM differences detected by Student's t-test and one-way ANOVA where appropriate.

Fig. 4. ERα Controls mitochondrial functionality and mitochondrial elimination by Parkin. (A) Maximal respiration as assessed by real-time respirometry (Seahorse Biosciences) was reduced in 3T3L1 adipocytes lacking ERα (n=6 per condition). (B-C) Fatty acid oxidation and esterification using ^{14}C palmitate in Esr1-KD and *Esr1* replete (Control Scr) 3T3L1 adipocytes. *Esr1* deletion (D-E) increases PINK1 and Parkin and (F-G) reduces Mfn2 protein levels in adipocytes (n=6 /condition). (H) Linear regression of the fold change in *Park2* expression and body fat % assessed by NMR from normal chow and HF/HS-fed male HMDP mice. (I) Esr1-KD promotes mitochondrial accumulation of Parkin and the mitochondrial stress protein p53, whereas (J) Esr1-AD (adenovirus) reduces p53 total protein and its mitochondrial localization to below that for Control (GFP-AD) (n=6 / condition). (K-L) Disruption of the p53 with PFTα at 10 and 50μM reduces Parkin accumulation in the mitochondrial fraction (n=3-6 per condition). (M-O) Adipose tissue Parkin deletion increases mtDNA copy number and this was paralleled by a reduction of white adipose tissue mass compared with the respective control mice (n=6 mice/condition). *, $P<0.05$ between the genotypes. Mean ± SEM differences detected by Student's t-test and one-way ANOVA where appropriate.

Fig. 5. ERα controls macroautophagy in white adipose tissue to regulate mitophagy. (A) Beclin, Atg5, 7, and 3, as well as LC3B processing (I to II) was increased in 3T3L1 adipocytes and (B-E) Beclin, Atg7, and LC3B processing were increased in WAT of FERKO vs. Control f/f mice (n=6 samples/genotype). Mean ± SEM differences detected by Student's t-test. *, $P<0.05$ between the genotypes.

Fig. 6. ERα controls UCP1 induction and substrate metabolism in brown adipocytes.
(A) *Esr1* and *Ucp1* expression, and (B) mtDNA copy number in brown adipose tissue (BAT) from male and female WT mice (n=5-6 mice/sex). (C) *Esr1* expression is induced in brown adipose tissue in female mice during cold challenge (closed bars; 5h, 4°C) vs. room temperature (open bars). (D) High fat diet feeding (HFD; black bars) and genetic obesity/leptin deficiency (Lep$^{Ob/+}$; gray bars) promote reduced expression of *Esr1*, *Polg1*, and *Polg2* compared with normal chow fed wildtype mice (open bars). (E) Confirmation of ERα deletion in BAT from female ERαKO^{BAT} mice (n=6/genotype). (F) Reduced Ucp1 expression in BAT from female ERαKO^{BAT} mice (closed bars) vs. Control$^{f/f}$ at room temperature, and impaired Ucp1 induction during cold challenge (closed bars; 5h, 4°C). (G) Increased body weight gain during early high fat diet feeding in ERαKO^{BAT} vs. Control$^{f/f}$ (n=5-6/genotype). (H) Increased white adipose tissue, inguinal (iWAT) and gonadal (gWAT), in ERαKO^{BAT} vs. Control$^{f/f}$ under normal chow (NC) and high fat diet (HFD)-feeding (n=5-6 mice / genotype). (I) Body temperature in ERαKO^{BAT} (closed square) vs. Control$^{f/f}$ (open circle) over time during cold challenge (5h, 4°C). (J) Increased lipid droplets in

BAT ERαKO^{BAT} (closed square) vs. Control$^{f/f}$ detected by histochemistry (n=3 / genotype). (K) Transmission Electron Microscopy showing mitochondrial architecture in ERαKO^{BAT} (closed square) vs. Control$^{f/f}$, with mitochondrial images quantified for (L) perimeter and (M) area. (N) mtDNA copy number determined by qPCR in BAT from male and female ERαKO^{BAT} (closed square) vs. Control$^{f/f}$ (n=5-6 mice/genotype). (O) Reduced Polg1 expression in BAT of ERαKO^{BAT} (closed bar) vs control (open bar), (P-S) Immunoblots and corresponding densitometry showing (Q) matched Parkin protein levels, and (R) reduced Dynamin related protein (Drp)1 total protein and (S) Drp1^{Ser600} phosphorylation in ERαKO^{BAT} (closed bars) vs. Control$^{f/f}$ (open bars) (n=6 mice / genotype). Data are means ± SEM. *, P<0.05.

Fig. 7. *Esr1* deletion alters substrate metabolism in BAT during cold stress.
(**A-B**) ^{18}FDG MicroCT-PET, performed on female Control$^{f/f}$ and ERαKO^{BAT} mice after 6h at room temperature or following a 6h cold challenge at 4°C, shows that BAT from ERαKO^{BAT} (closed bars) mice utilizes more glucose than Control$^{f/f}$ (open bars). (**C**) The higher glucose reliance in ERαKO^{BAT} is further increased during cold stress when fatty acid oxidation is typically maximized and this caused a marked reduction in blood glucose by ~50% during thermal challenge compared with Control$^{f/f}$. Data are means ± SEM, and mean differences were detected by student's t-test or one-way ANOVA where appropriate. *, P<0.05.
(D) Schematic overview of the mechanisms by which ERα controls adipocyte metabolism and adiposity. Collectively our findings show that the ERα target gene *Polg1* is reduced in expression in both white and brown adipocytes in the context of Esr1 KO. *Polg1* via its role in the control of mtDNA replication, is intimately associated with fission-fusion-mitophagy dynamics. However the precise feedback from *Polg1* to the enzymes that control mitochondrial remodeling and turnover appears to be cell specific. In white adipose tissue Esr1 deletion reduces mtDNA copy number by increased mitophagic signaling via Parkin. In brown adipose tissue, Esr1 deletion impairs mitochondrial fission via reduced Drp1 signaling and this prevents lipid droplet lipolysis, fatty acid utilization, and Ucp1 induction during cold exposure. In both mouse models, a loss of ERα from white or brown adipose tissue promotes increased lipid deposition in BAT and increased white adipose tissue accumulation. Our findings support the notion that the central mechanism by which ERα restrains adiposity is by controlling mitochondrial content and metabolism in white and brown adipocytes.

Abbreviations
18S – 18S ribosomal RNA
Acta1 – Actin1 Alpha 1
AMPKA – Protein Kinase AMPK-Activated Catalytic Subunit Alpha 1
Atg10 – Autophagy Related 10
Atg12 – Autophagy Related 12
Atg3 – Autophagy Related 3
Atg5 – Autophagy Related 5
Atg7 – Autophagy Related 7
Cebpa – CCAAT/Enhancer Binding Protein Alpha
CII-SDHB – Succinate Dehydrogenase Complex Iron Sulfur Subunit B
CI-NDUFB8 – NADH:Ubiquinone Oxidoreductase Subunit B8
CIV-mtCO1 – Mitochondrially Encoded Cytochrome C Oxidase I
Col6A1 – Collagen Type VI Alpha 1 Chain
Ctnnb1 – Catenin Beta 1
CV-ATP5a – ATP Synthase F1 Subunit Alpha
Drp1 – Dynamin Related Protein 1 (DNM1L)
Esr1 – Estrogen Receptor 1

Fis1 – Fission, Mitochondrial 1
Foxo1 – Forkhead Box O1
Foxo4 – Forkhead Box O4
Gast – Gastrocnemius Muscle
Gfm2 – G Elongation Factor Mitochondrial 2
gWAT – Gonadal White Adipose Tissue
Itgam – Integrin Subunit Alpha M
iWAT – Inguinal White Adipose Tissue
LC3B – Mirotubule Associated Protein 1 Light Chain 3 Beta (MAPLC3B)
MFF – Mitochondrial Fission Factor
MFN1 – Mitofusin 1
MFN2 – Mitofusin 2
Mgme1 – Mitochondrial Genome Maintenance Exonuclease 1
mtCO2 – Mitochondrially Encoded Cytochrome C Oxidase II
mtDNA – Mitochondrial DNA
Nfkb1 – Nuclear Factor Kappa B Subunit 1
Nfkbia – NFKB Inhibitor Alpha
NRF1 – Nuclear Respiratory Factor 1
NRF2 – Nuclear Respiratory Factor 2
Opa1 – Optic Atrophy Protein 1
Park2 – Parkinson Disease 2 (Parkin)
Peo1 – Twinkle mtDNA Helicase
PGC1α - Peroxisome proliferator-activated receptor gamma coactivator 1-alpha
Pink1 – PTEN Induced Putative Kinase 1
PKA – Protein Kinase CAMPK-Acticated Catalytic Subunit Alpha
PolG – DNA Polymerase Gamma, Catalytic Subunit
PolGII – DNA Polymerase Gamma 2, Accessory Subunit
Polrmt – RNA Polymerase Mitochondrial
Pparg – Peroxisome Proliferator Activated Receptor Gamma
Ppia – Peptidylprolyl isomerase A
Quad – Quadriceps Muscle
SIII-UQCRC2 – Ubiquinol-Cytochrome C Reductase Core Protein 2
TFAM – Mitochondrial Transcription Factor A

REFERENCES

1. A. Kautzky-Willer, J. Harreiter, G. Pacini, Sex and Gender Differences in Risk, Pathophysiology and Complications of Type 2 Diabetes Mellitus. *Endocr Rev* **37**, 278-316 (2016).
2. G. A. Greendale *et al.*, Changes in body composition and weight during the menopause transition. *JCI Insight* **4**, (2019).
3. S. Heinonen *et al.*, Mitochondria-related transcriptional signature is downregulated in adipocytes in obesity: a study of young healthy MZ twins. *Diabetologia* **60**, 169-181 (2017).
4. X. Yin *et al.*, Adipocyte mitochondrial function is reduced in human obesity independent of fat cell size. *J Clin Endocrinol Metab* **99**, E209-216 (2014).
5. R. Zamora-Mendoza *et al.*, Dysregulation of mitochondrial function and biogenesis modulators in adipose tissue of obese children. *Int J Obes (Lond)* **42**, 618-624 (2018).
6. F. Norheim *et al.*, Gene-by-Sex Interactions in Mitochondrial Functions and Cardio-Metabolic Traits. *Cell Metab* **29**, 932-949 e934 (2019).

7. M. Nilsson *et al.*, Oestrogen receptor alpha gene expression levels are reduced in obese compared to normal weight females. *Int J Obes (Lond)* **31**, 900-907 (2007).
8. B. G. Drew *et al.*, Estrogen receptor (ER)alpha-regulated lipocalin 2 expression in adipose tissue links obesity with breast cancer progression. *J Biol Chem* **290**, 5566-5581 (2015).
9. D. Ricquier, J. C. Kader, Mitochondrial protein alteration in active brown fat: a soidum dodecyl sulfate-polyacrylamide gel electrophoretic study. *Biochem Biophys Res Commun* **73**, 577-583 (1976).
10. M. Hibi *et al.*, Brown adipose tissue is involved in diet-induced thermogenesis and whole-body fat utilization in healthy humans. *Int J Obes (Lond)* **40**, 1655-1661 (2016).
11. M. Klingenberg, UCP1 - A sophisticated energy valve. *Biochimie* **134**, 19-27 (2017).
12. A. A. van der Lans *et al.*, Cold acclimation recruits human brown fat and increases nonshivering thermogenesis. *J Clin Invest* **123**, 3395-3403 (2013).
13. J. Nedergaard *et al.*, UCP1: the only protein able to mediate adaptive non-shivering thermogenesis and metabolic inefficiency. *Biochim Biophys Acta* **1504**, 82-106 (2001).
14. J. Nedergaard *et al.*, Life without UCP1: mitochondrial, cellular and organismal characteristics of the UCP1-ablated mice. *Biochem Soc Trans* **29**, 756-763 (2001).
15. V. Golozoubova *et al.*, Only UCP1 can mediate adaptive nonshivering thermogenesis in the cold. *FASEB J* **15**, 2048-2050 (2001).
16. M. Calderon-Dominguez *et al.*, Fatty acid metabolism and the basis of brown adipose tissue function. *Adipocyte* **5**, 98-118 (2016).
17. A. M. Cypess *et al.*, Identification and importance of brown adipose tissue in adult humans. *N Engl J Med* **360**, 1509-1517 (2009).
18. J. C. van den Beukel *et al.*, Women have more potential to induce browning of perirenal adipose tissue than men. *Obesity (Silver Spring)* **23**, 1671-1679 (2015).
19. S. M. Al-Qahtani *et al.*, 17beta-Estradiol suppresses visceral adipogenesis and activates brown adipose tissue-specific gene expression. *Horm Mol Biol Clin Investig* **29**, 13-26 (2017).
20. V. Ribas *et al.*, Skeletal muscle action of estrogen receptor alpha is critical for the maintenance of mitochondrial function and metabolic homeostasis in females. *Sci Transl Med* **8**, 334ra354 (2016).
21. Z. Zhou *et al.*, Estrogen receptor alpha protects pancreatic beta-cells from apoptosis by preserving mitochondrial function and suppressing endoplasmic reticulum stress. *J Biol Chem* **293**, 4735-4751 (2018).
22. A. Lindinger *et al.*, Mitochondrial DNA content in human omental adipose tissue. *Obes Surg* **20**, 84-92 (2010).
23. A. Hoshino *et al.*, Inhibition of p53 preserves Parkin-mediated mitophagy and pancreatic beta-cell function in diabetes. *Proc Natl Acad Sci U S A* **111**, 3116-3121 (2014).
24. W. Fu, Y. Liu, C. Sun, H. Yin, Transient p53 inhibition sensitizes aged white adipose tissue for beige adipocyte recruitment by blocking mitophagy. *FASEB J*, fj201800577R (2018).
25. T. Minamino *et al.*, A crucial role for adipose tissue p53 in the regulation of insulin resistance. *Nat Med* **15**, 1082-1087 (2009).
26. J. Krstic, I. Reinisch, M. Schupp, T. J. Schulz, A. Prokesch, p53 Functions in Adipose Tissue Metabolism and Homeostasis. *Int J Mol Sci* **19**, (2018).
27. I. Shimizu *et al.*, p53-induced adipose tissue inflammation is critically involved in the development of insulin resistance in heart failure. *Cell Metab* **15**, 51-64 (2012).
28. X. J. Han *et al.*, CaM kinase I alpha-induced phosphorylation of Drp1 regulates mitochondrial morphology. *J Cell Biol* **182**, 573-585 (2008).

29. J. D. Wikstrom *et al.*, Hormone-induced mitochondrial fission is utilized by brown adipocytes as an amplification pathway for energy expenditure. *EMBO J* **33**, 418-436 (2014).
30. K. Mahdaviani *et al.*, Mfn2 deletion in brown adipose tissue protects from insulin resistance and impairs thermogenesis. *EMBO Rep* **18**, 1123-1138 (2017).
31. D. F. Pisani *et al.*, Mitochondrial fission is associated with UCP1 activity in human brite/beige adipocytes. *Mol Metab* **7**, 35-44 (2018).
32. H. J. Choo *et al.*, Mitochondria are impaired in the adipocytes of type 2 diabetic mice. *Diabetologia* **49**, 784-791 (2006).
33. S. D. Konduri *et al.*, Mechanisms of estrogen receptor antagonism toward p53 and its implications in breast cancer therapeutic response and stem cell regulation. *Proc Natl Acad Sci U S A* **107**, 15081-15086 (2010).
34. N. Yahagi *et al.*, p53 Activation in adipocytes of obese mice. *J Biol Chem* **278**, 25395-25400 (2003).
35. J. Naukkarinen *et al.*, Characterising metabolically healthy obesity in weight-discordant monozygotic twins. *Diabetologia* **57**, 167-176 (2014).
36. D. Taylor, R. A. Gottlieb, Parkin-mediated mitophagy is downregulated in browning of white adipose tissue. *Obesity (Silver Spring)* **25**, 704-712 (2017).
37. K. Y. Kim *et al.*, Parkin is a lipid-responsive regulator of fat uptake in mice and mutant human cells. *J Clin Invest* **121**, 3701-3712 (2011).
38. X. Lu *et al.*, Mitophagy controls beige adipocyte maintenance through a Parkin-dependent and UCP1-independent mechanism. *Sci Signal* **11**, (2018).
39. R. S. Santos *et al.*, Activation of estrogen receptor alpha induces beiging of adipocytes. *Mol Metab*, (2018).
40. F. Forner *et al.*, Proteome differences between brown and white fat mitochondria reveal specialized metabolic functions. *Cell Metab* **10**, 324-335 (2009).
41. J. A. Timmons *et al.*, Myogenic gene expression signature establishes that brown and white adipocytes originate from distinct cell lineages. *Proc Natl Acad Sci U S A* **104**, 4401-4406 (2007).
42. S. Kajimura *et al.*, Initiation of myoblast to brown fat switch by a PRDM16-C/EBP-beta transcriptional complex. *Nature* **460**, 1154-1158 (2009).
43. P. Seale, S. Kajimura, B. M. Spiegelman, Transcriptional control of brown adipocyte development and physiological function--of mice and men. *Genes Dev* **23**, 788-797 (2009).
44. C. R. Chang, C. Blackstone, Drp1 phosphorylation and mitochondrial regulation. *EMBO Rep* **8**, 1088-1089; author reply 1089-1090 (2007).
45. C. R. Chang, C. Blackstone, Cyclic AMP-dependent protein kinase phosphorylation of Drp1 regulates its GTPase activity and mitochondrial morphology. *J Biol Chem* **282**, 21583-21587 (2007).
46. V. Barquissau *et al.*, White-to-brite conversion in human adipocytes promotes metabolic reprogramming towards fatty acid anabolic and catabolic pathways. *Mol Metab* **5**, 352-365 (2016).
47. S. C. Lewis, L. F. Uchiyama, J. Nunnari, ER-mitochondria contacts couple mtDNA synthesis with mitochondrial division in human cells. *Science* **353**, aaf5549 (2016).
48. G. Twig, B. Hyde, O. S. Shirihai, Mitochondrial fusion, fission and autophagy as a quality control axis: the bioenergetic view. *Biochim Biophys Acta* **1777**, 1092-1097 (2008).
49. G. Twig *et al.*, Fission and selective fusion govern mitochondrial segregation and elimination by autophagy. *EMBO J* **27**, 433-446 (2008).
50. E. Grundberg *et al.*, Mapping cis- and trans-regulatory effects across multiple tissues in twins. *Nat Genet* **44**, 1084-1089 (2012).

51. C. A. Glastonbury *et al.*, Adiposity-Dependent Regulatory Effects on Multi-tissue Transcriptomes. *Am J Hum Genet* **99**, 567-579 (2016).
52. A. Buil *et al.*, Gene-gene and gene-environment interactions detected by transcriptome sequence analysis in twins. *Nat Genet* **47**, 88-91 (2015).
53. S. Lee *et al.*, Skeletal muscle phosphatidylcholine and phosphatidylethanolamine respond to exercise and influence insulin sensitivity in men. *Sci Rep* **8**, 6531 (2018).
54. Y. Li *et al.*, Subsarcolemmal lipid droplet responses to a combined endurance and strength exercise intervention. *Physiol Rep* **2**, (2014).
55. T. M. Langleite *et al.*, Insulin sensitivity, body composition and adipose depots following 12 w combined endurance and strength training in dysglycemic and normoglycemic sedentary men. *Arch Physiol Biochem* **122**, 167-179 (2016).
56. F. Norheim *et al.*, The effects of acute and chronic exercise on PGC-1alpha, irisin and browning of subcutaneous adipose tissue in humans. *FEBS J* **281**, 739-749 (2014).
57. J. Vangipurapu *et al.*, Association of indices of liver and adipocyte insulin resistance with 19 confirmed susceptibility loci for type 2 diabetes in 6,733 non-diabetic Finnish men. *Diabetologia* **54**, 563-571 (2011).
58. B. G. Drew *et al.*, HSP72 is a mitochondrial stress sensor critical for Parkin action, oxidative metabolism, and insulin sensitivity in skeletal muscle. *Diabetes* **63**, 1488-1505 (2014).
59. S. Lee *et al.*, Effect of energy restriction and physical exercise intervention on phenotypic flexibility as examined by transcriptomics analyses of mRNA from adipose tissue and whole body magnetic resonance imaging. *Physiol Rep* **4**, (2016).
60. J. Wanagat, Z. Cao, P. Pathare, J. M. Aiken, Mitochondrial DNA deletion mutations colocalize with segmental electron transport system abnormalities, muscle fiber atrophy, fiber splitting, and oxidative damage in sarcopenia. *FASEB J* **15**, 322-332 (2001).
61. J. M. Graham, Purification of a crude mitochondrial fraction by density-gradient centrifugation. *Curr Protoc Cell Biol* **Chapter 3**, Unit 3 4 (2001).
62. J. Collins *et al.*, Production of diverse PET probes with limited resources: 24 (18)F-labeled compounds prepared with a single radiosynthesizer. *Proc Natl Acad Sci U S A* **114**, 11309-11314 (2017).
63. C. A. Schneider, W. S. Rasband, K. W. Eliceiri, NIH Image to ImageJ: 25 years of image analysis. *Nat Methods* **9**, 671-675 (2012).

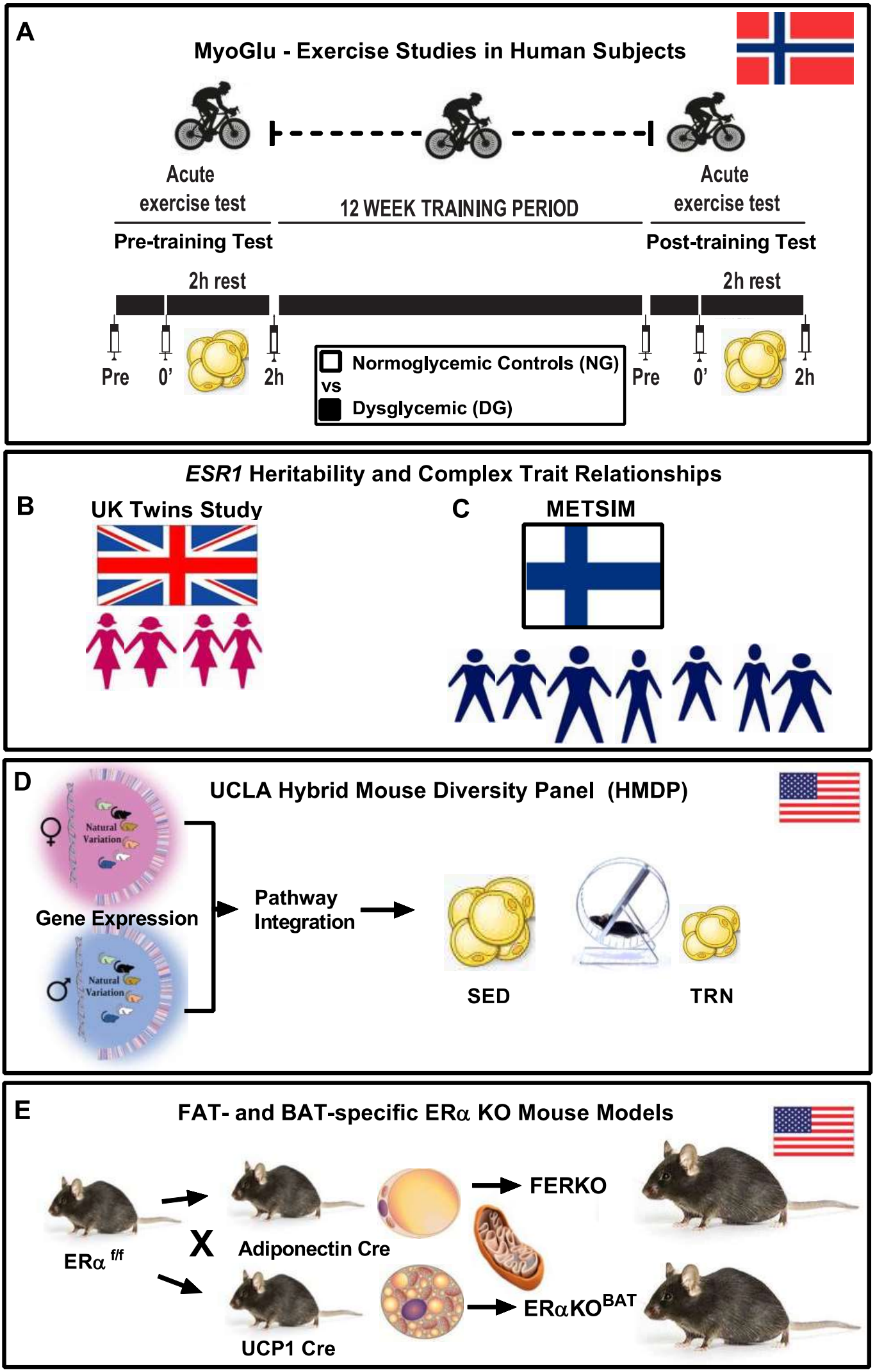

Figure 1. Zhou et al.

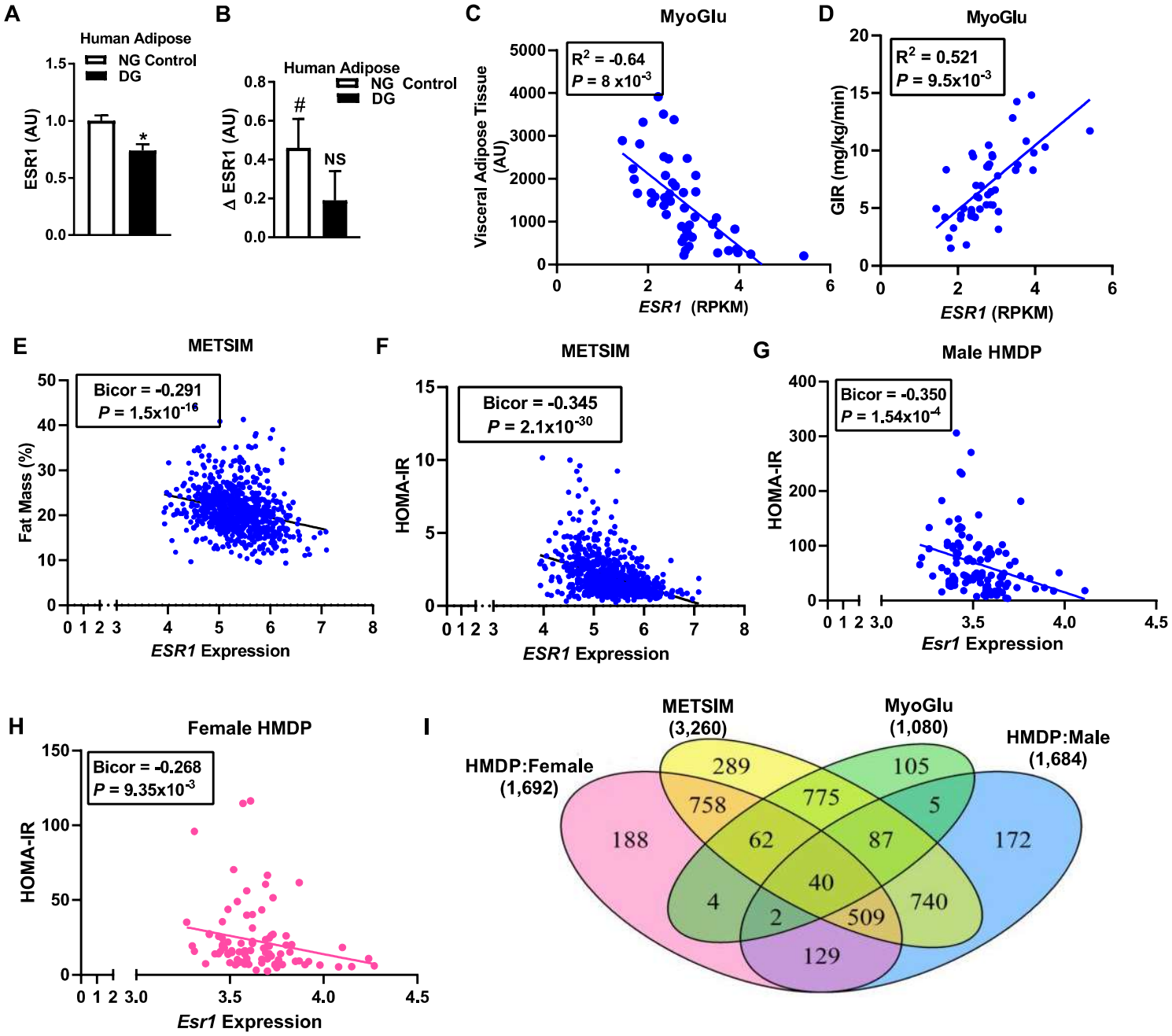

Figure 2. Zhou et al.

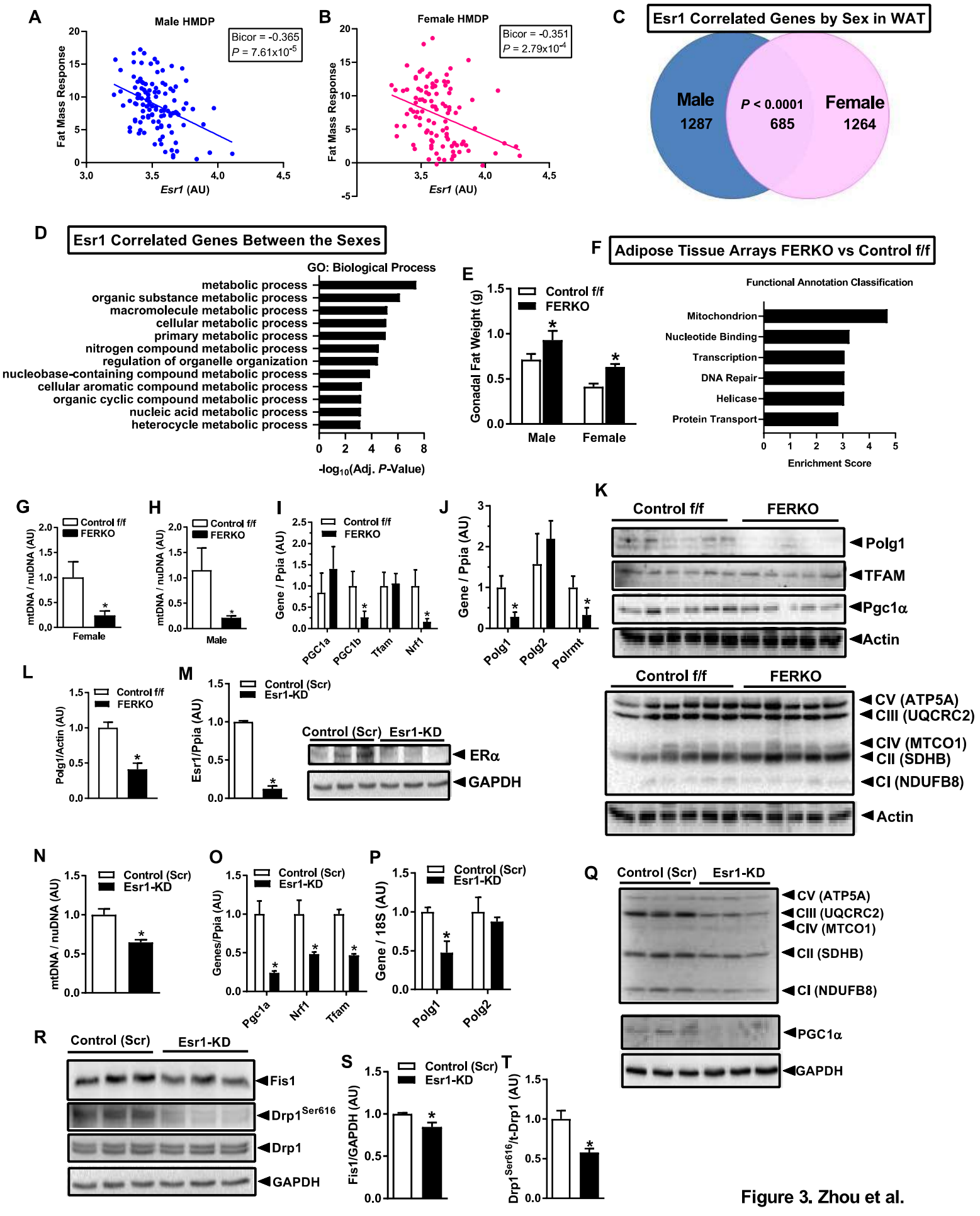

Figure 3. Zhou et al.

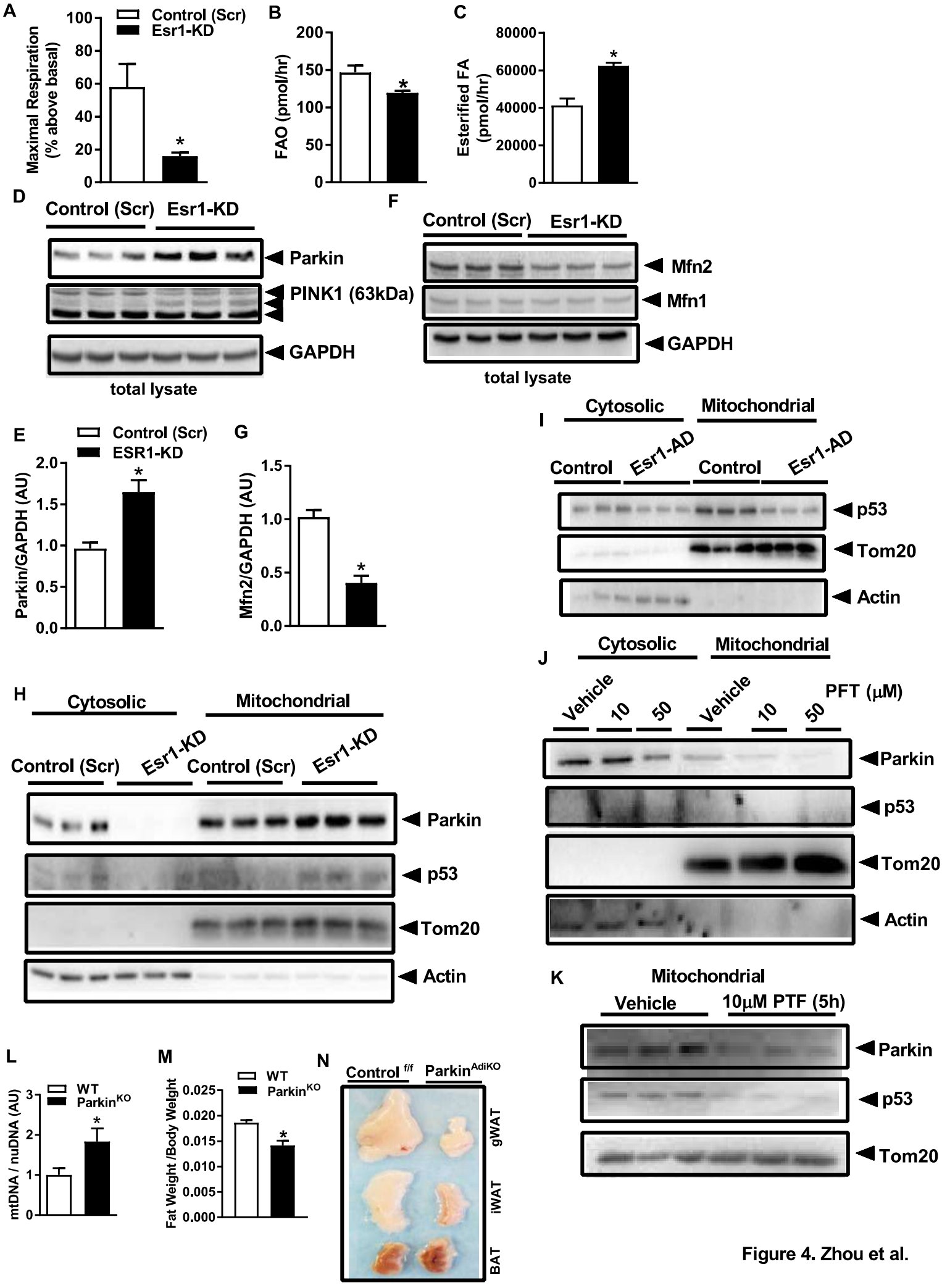

Figure 4. Zhou et al.

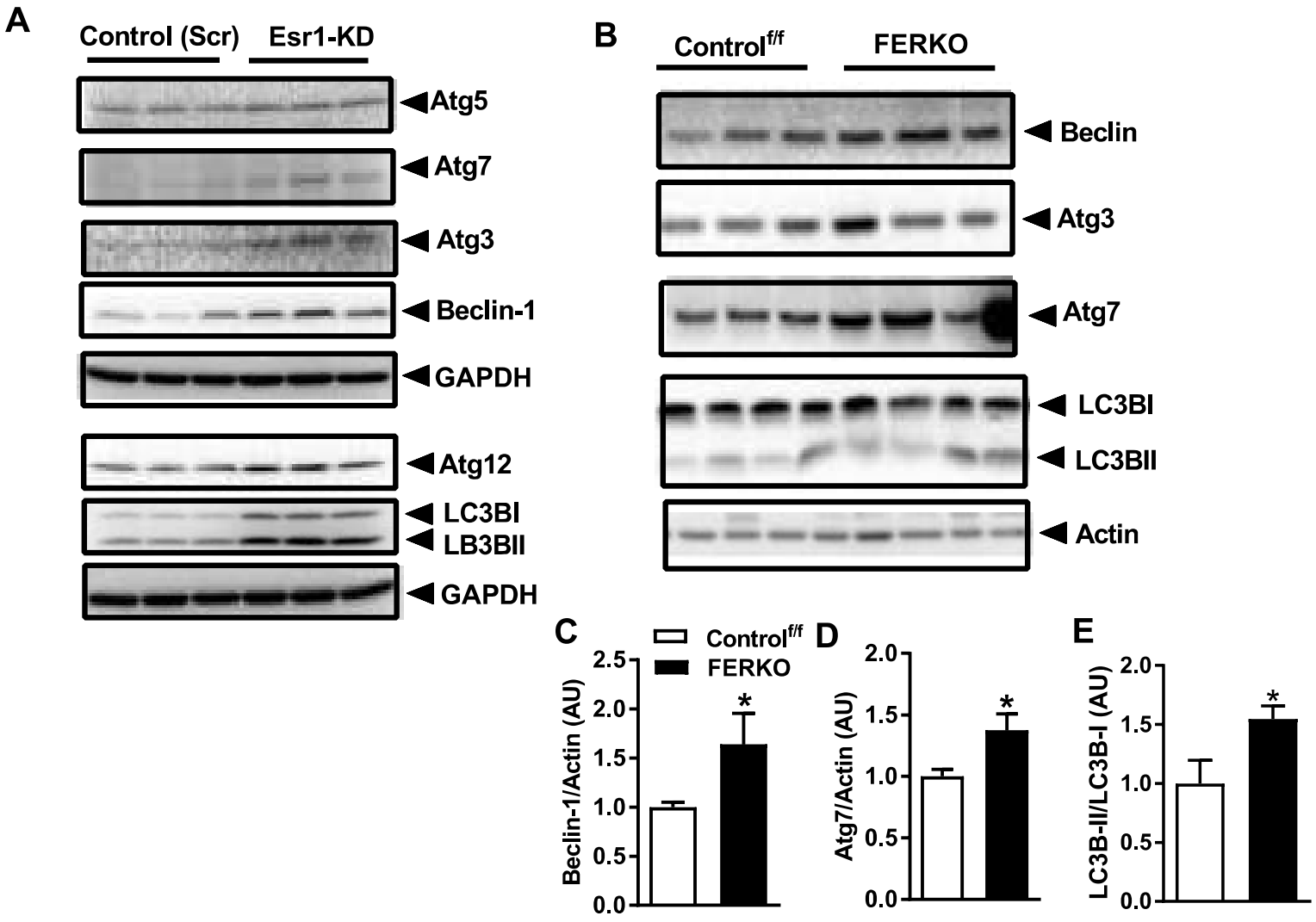

Figure 5. Zhou et al.

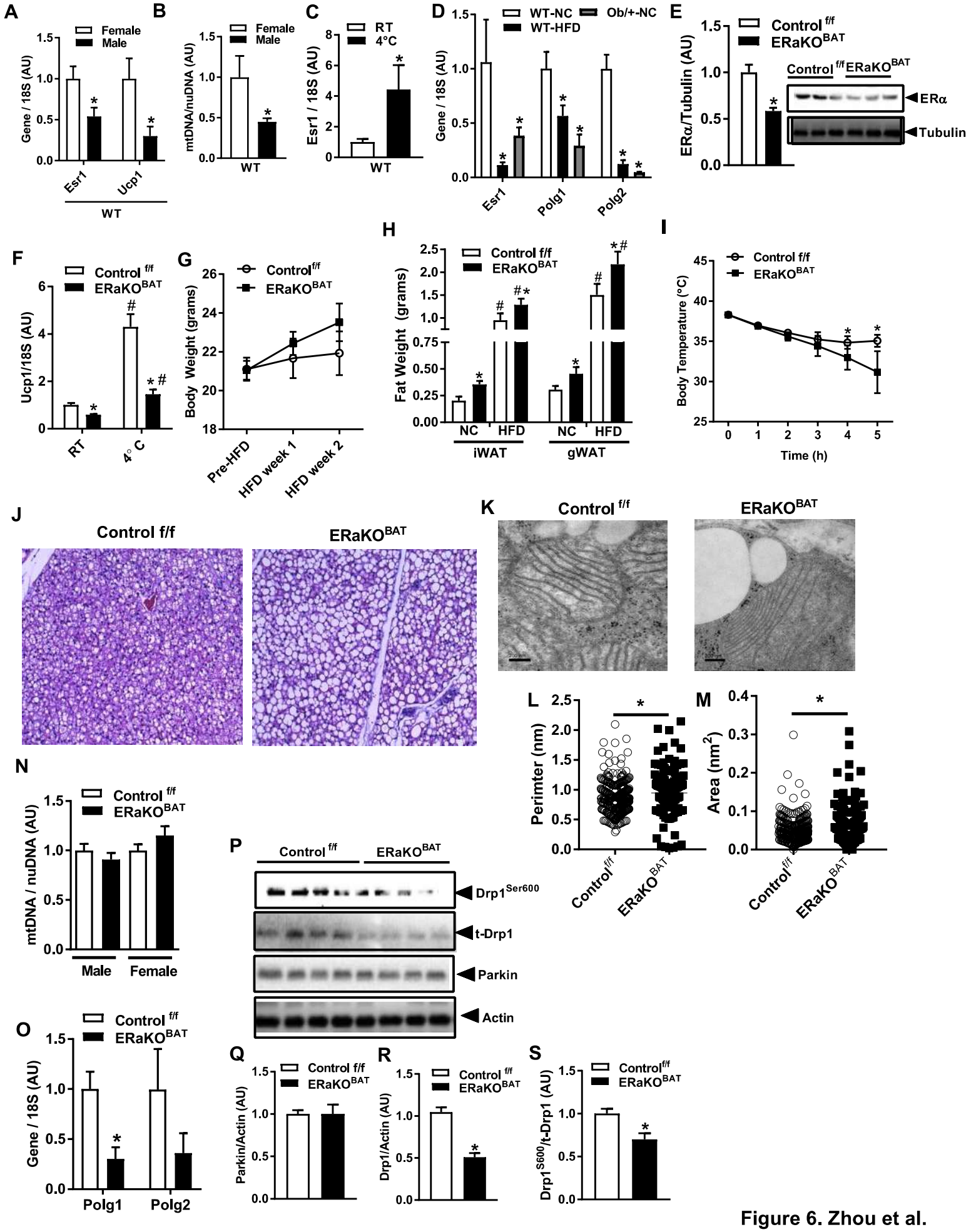

Figure 6. Zhou et al.

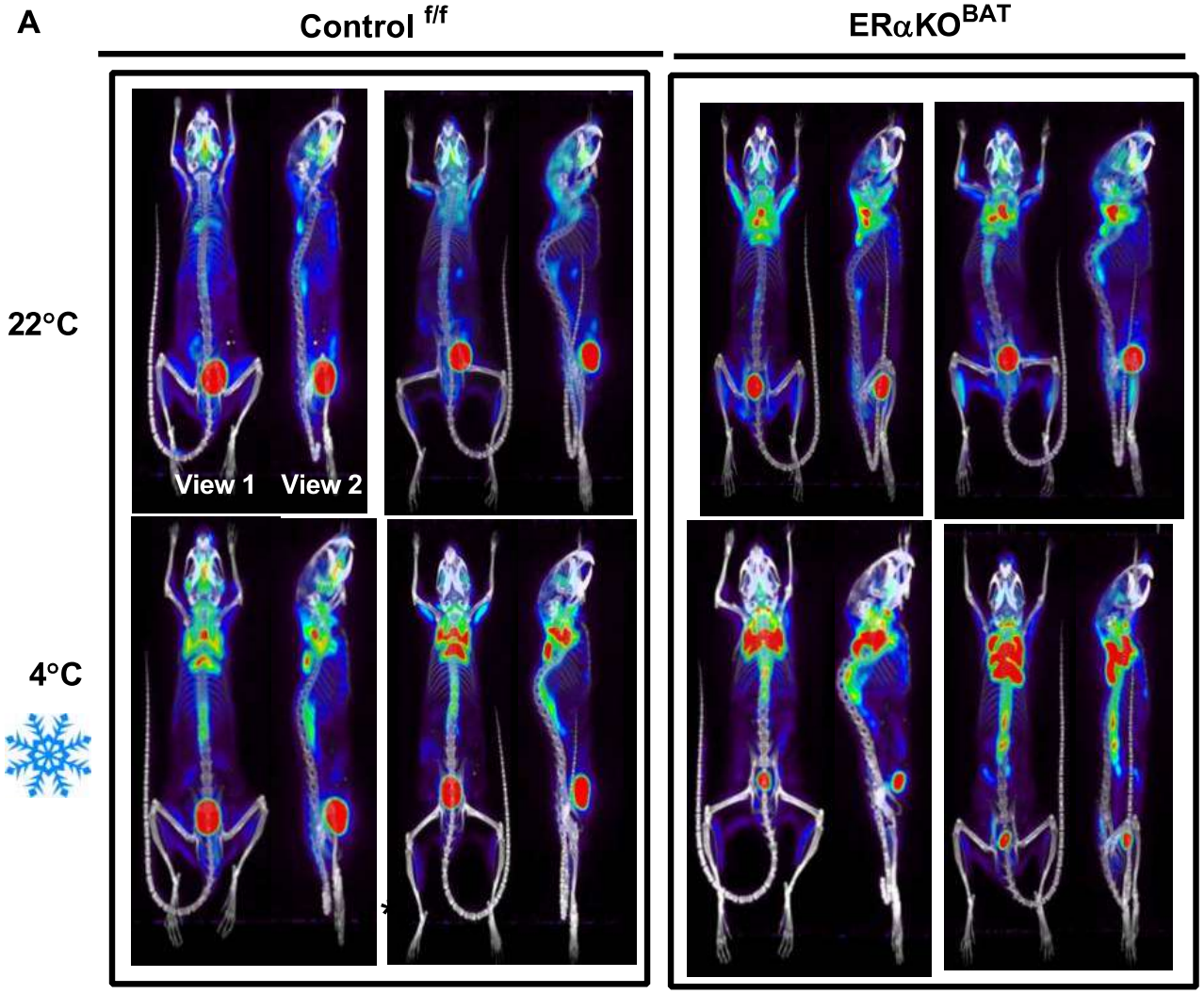

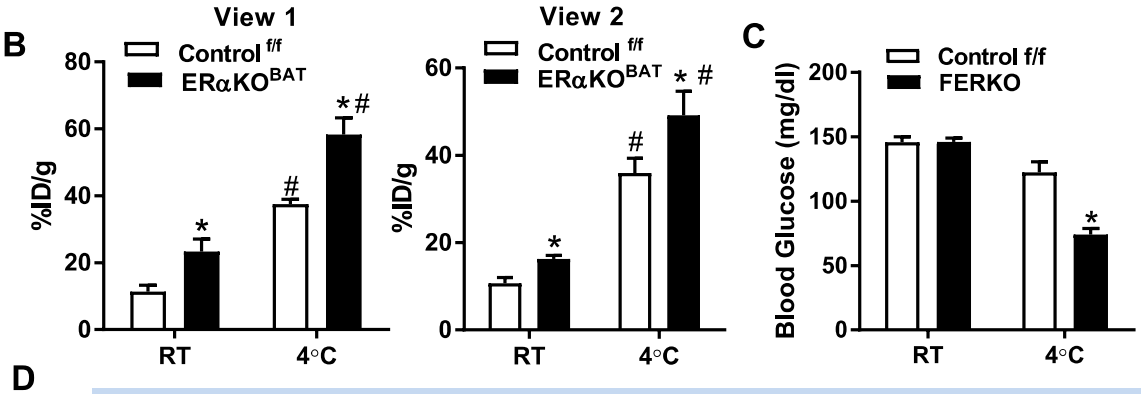

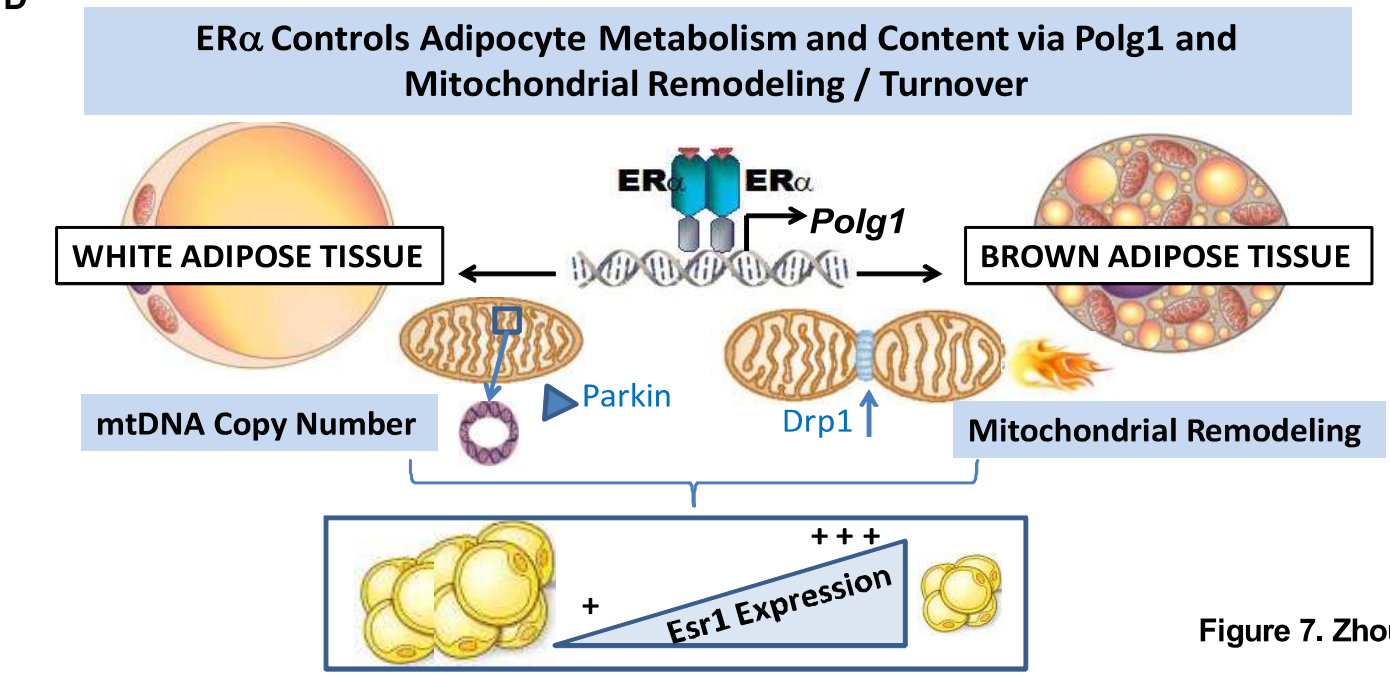

Figure 7. Zhou et al.

Supplemental Information

supplemental table s1. List of strains studied from the Hybrid Mouse Diversity Panel (HMDP).

supplemental table s2. List of qPCR primers used to assess gene expression in adipose tissue from studies performed on wildtype C57BL/6J mice, as well as Control$^{f/f}$, FERKO, and ERaKO^{BAT} mice.

supplemental table 1.
HMDP Strains: Male and female mice (N=4 mice/strain)

A/J	BXD44/RwwJ	BXH20/KccJ
AKR/J	BXD45/RwwJ	BXH22/KccJ
AXB12/PgnJ	BXD48/RwwJ	BXH8/TyJ
AXB15/PgnJ	BXD49/RwwJ	BXH9/TyJ
AXB19/PgnJ	BXD5/TyJ	C3H/HeJ
AXB19a/PgnJ	BXD50/RwwJ	C57BL/6J
AXB19b/PgnJ	BXD51/RwwJ	C57BLKS/J
BALB/cJ	BXD55/RwwJ	C58/J
BUB/BnJ	BXD56/RwwJ	CBA/J
BXA11/PgnJ	BXD6/TyJ	CE/J
BXA14/PgnJ	BXD60/RwwJ	CXB11/HiAJ
BXA16/PgnJ	BXD61/RwwJ	CXB12/HiAJ
BXA2/PgnJ	BXD62/RwwJ	CXB13/HiAJ
BXA24/PgnJ	BXD64/RwwJ	CXB4/ByJ
BXA4/PgnJ	BXD66/RwwJ	CXB6/ByJ
BXA7/PgnJ	BXD68/RwwJ	CXB7/ByJ
BXA8/PgnJ	BXD70/RwwJ	DBA/2J
BXD12/TyJ	BXD71/RwwJ	FVB/NJ
BXD14/TyJ	BXD73/RwwJ	KK/HlJ
BXD15/TyJ	BXD74/RwwJ	MA/MyJ
BXD19/TyJ	BXD75/RwwJ	NOD/ShiLtJ
BXD20/TyJ	BXD79/RwwJ	NZW/LacJ
BXD21/TyJ	BXD84/RwwJ	PL/J
BXD31/TyJ	BXD85/RwwJ	RIIIS/J
BXD34/TyJ	BXD86/RwwJ	SEA/GnJ
BXD38/TyJ	BXD87/RwwJ	SJL/J
BXD40/TyJ	BXD9/TyJ	SM/J
BXD43/RwwJ	BXH19/TyJ	SWR/J

supplemental table s2

Gene Symbol	Forward (5' -> 3')	Reverse (5' -> 3')
18S	CGCCGCTAGAGGTGAAATTCT	CGAACCTCCGACTTTCGTTCT
Acta1	CCAGCCTTCCTTTATCGGTATG	CGGTCAGCGATACCAGGG
Atg12	CCACAGCCCATTTCTTTGTT	GAAACAGCCACCCCAGAG
Atg3	ATTCTTCCCCTGTAGCCCAT	GAAGTGGCCGAGTACCTGAC
Atg5	ACAGCTTCTGGATGAAAGGC	TGGGACTGCAGAATGACAGA
Atg7	GCCAGGTACTCCTGAGCTGT	ACTTGACCGGTCTTACCCTG
Beclin-1	CCCCGATCAGAGTGAAGCTA	AGGAGAGACCCAGGAGGAAG
Ctnnb1	CAGCTTGAGTAGCCATTGTCC	GAGCCGTCAGTGCAGGAG
Cav1	ATGTCTGGGGGCAAATACGTG	CGCGTCATACACTTGCTTCT
Col6A1	TCGGTCACCACGATCAAGTA	CAAGTACTTCGGGAAAGGCA
DNM1L	CGTGGACTAGCTGCAGAATG	TGCCTCAGATCGTCGTAGTG
Esr1	GCCAGAATGGCCGAGAGAG	CCCCATAATGGTAGCCAGAGG
Gfm2	ACCGTCCAACACCCTCAAG	AAGAACGAGAAAGGGGCATT
Itgam	CCCCAATTACGTAGCGAATG	TGCTGCGAAGATCCTAGTTG
MAPLC3B	AATCACTGGGATCTTGGTGG	AGTCAGATCGTCTGGCTCG
mtCO2	CTACAAGACGCCACAT	GAGAGGGGAGAGCAAT
Fis1	AGGAGCTGGAACGCCTGATTGATA	AGGATTTGGACTTGGAGACAGCCA
MFF	GCAGTTGGCAGGCTAAAAAG	TCAGGTAGCATATGGGGAGG
Mgme1	TGTTAGGTTCTCCTGGGGTG	TTTGGAGAGGTGGAAAGAGC
MrpI9	GCAACCACCACACCAAGATT	GATCCAGACAAAGGCAGGAG
Mrps2	CGGTGAAGTTCAAAGCCAGT	CCGAGTACACCTGGGACATAA
Mrps24	GGAAAGGTGCCCATCATAAA	ACTACATCGCACACCGAAAG
MFN2	ATTGATCACGGTGCTCTTCC	GTCCTGGACGTCAAAGGGTA
MFN1	GCTTCCGACGGACTTACAAC	TGAATAACCGTTGGGATGCT
Myod1	AGGCCGTGGCAGCGA	GCTGTAATCCATCATGCCATCA
Myog	CAACCAGGAGGAGCGCGATCTCCG	AGGCGCTGTGGGAGTTGCATTCACT
Myh4	AGCTCGTGCTGGATCTTACG	GCAGGACTTGGTGGACAAAC
Myh6	CTTCATCCATGGCCAATTCT	GCGCATTGAGTTCAAGAAGA
Myh7	CTCAACTGGGAAGAGCATCCA	CCTCCAGCAAACTCTGGAGGC
NRF1	GAACTGCCAACCACAGTCAC	CGTCTGGATGGTCATTTCAC
Opa1	TCCTGGTGAAGAGCTTCAATG	TTTGCAGAAGACGGTGAGAA
Park2	ATCGACCTCCACTGGGAAG	GCGTAGGTCCTTCTCGACC
Park7	AACACACCCACTGGCTAAGG	GTGCCTCCACAATGGCTAGT
Ppia	AGCCAAATCCTTTCTCTCCAG	CACCGTGTTCTTCGACATCA
PGC1α	TGAGGACCGCTAGCAAGTTT	TGAAGTGGTGTAGCGACCAA
PolG	TAGCTGGCTGGTCCAAGAGT	CGACGTGGAGGTCTGCTT
PolGII	CCGTTTTCCAGCGTAGTCTC	TTCTGTGTGGCCTGGCTATT
Polrmt	CTCATCTCAGGTGTGCCCTC	TCTGCAGCTCAAGAAGGAGC
Peo1	GCCCAGTCACCAGTTTCCTA	ACTCTGGTCATTCACCCTCG
Ppp3cc	GCGATTGATCCCAAGTTGTC	TGCCCTCCTTCATGAGATGT

Pink1	GGATGTCGTCCTGAAGGGAG	GCTTCGCTGGAGGAACCTG
Rcan	TGTGGCAAACGATGATGTCT	GCAGATAAGGGGTTGCTGAA
SQSTM1	TTTCTGGGGTAGTGGGTGTC	CTGAAGAATGTGGGGGAGAG
S1pr3	TCTTAGCTGAGACACGGCAG	TCAGGGAACAATTGGGAGAG
SDHA	TACTACAGCCCCAAGTCT	TGGACCCATCTTCTATGC
TFAM	AGCTTGTAAATGAGGCTTGGA	AGATGTCTCCGGATCGTTTC
Tnni1	CCCTACTGGGCTCTAAGCACA	GCCTCCACATTCTTCCTCCA
Tnni2	CTGTCAGAACACTGCCCGC	GCTCCTTGCTGCTCTTCTGC
Ulk1	TAGTCAGCCAGGTCTCCACC	CTGCTGGGAAAGGAAATCAA
Vegfa	AATGCTTTCTCCGCTCTGAA	CTCACCAAAGCCAGCACATA